SCIENCE CHINA
Technological Sciences

•Article•

https://doi.org/10.1007/s11431-019-1439-2

Comparison of settlement behaviors of high-food-waste-content (HFWC) and low-food-waste-content (LFWC) MSWs and assessment of their prediction models

XU Hui[1,2], QIU HaoLei[1,3], ZHU Guang[1], ZHAN LiangTong[2], ZHANG ZhenYing[1], XU XiaoBing[4], CHEN YunMin[2] & WANG YuZe[5*]

[1] *School of Civil Engineering and Architecture, Zhejiang Sci-Tech University, Hangzhou 310018, China;*
[2] *MOE Key Laboratory of Soft Soils and Geoenvironmental Engineering, Zhejiang University, Hangzhou 310058, China;*
[3] *Key Laboratory of Ministry of Education for Geomechanics and Embankment Engineering, Hohai University, Nanjing 210098, China;*
[4] *Institute of Geotechnical Engineering, Zhejiang University of Technology, Hangzhou 310014, China;*
[5] *Department of Engineering, Durham University, Lower Mountjoy, South Road, Durham DH1 3LE, UK*

Received May 22, 2019; accepted September 2, 2019; published online November 19, 2019

Settlement behaviors of high-food-waste-content (HFWC) and low-food-waste-content (LFWC) municipal solid wastes (MSWs) respectively from developing and developed countries were characterized and compared based on a great number of experimental datasets from references. Fresh HFWC-MSW generally has larger primary compression ratio compared to fresh LFWC-MSW, due to the release of a large amount of intra-particle water contained in food waste under additional stresses. The slopes of strain-logarithmic time curves with respect to the three secondary compression phases are characterized as "slight-steep-slight" for LFWC-MSW and "moderate-moderate-slight" for HFWC-MSW. It is difficult to distinguish the first two phases of the secondary compression in strain-logarithmic time curves for HFWC-MSW. The entropy method was built to evaluate the performance and applicability of nine published settlement models based on the settlement datasets of four large-scale experiments. The computational simplicity, the fitting performance, the prediction performance and the parametric stability were taken as the four criterions in the entropy method. Based on the evaluation results, the models proposed by Sowers et al. (1973) and Gourc et al. (2010) are recommended for predicting settlement at LFWC-MSW landfills, while the hyperbolic model and the Chen et al. (2010) model are recommended for HFWC-MSW landfills.

municipal solid waste (MSW), settlement behaviour, high food waste content (HFWC), low food waste content (LFWC), entropy method, settlement model assessment

Citation: Xu H, Qiu H L, Zhu G, et al. Comparison of settlement behaviors of high-food-waste-content (HFWC) and low-food-waste-content (LFWC) MSWs and assessment of their prediction models. Sci China Tech Sci, 2019, 62, https://doi.org/10.1007/s11431-019-1439-2

1 Introduction

Municipal solid waste (MSW) has normally been disposed in landfills in both developed and developing countries [1–6]. MSWs may settle in landfills when subjected to vertical stress or/and bio-degradation, and therefore the estimation of the settlement behavior of MSWs is essential for improving the utilization capacity of landfills, rationalizing landfill operations and providing information for site reclamation [7–9]. MSW settlement mainly consists of primary compression and secondary compression [1,10–16]. Primary compression is caused by the compaction of void space and solid particles of MSW, as well as by the consolidation of the skeleton of MSW due to the dissipation of pore water pressure. Secondary compression includes: (1) mechanical creep, which is led by the yield, slippage and reorientation of the

*Corresponding author (email: yuze.wang@durham.ac.uk)

solid particles; and (2) bio-induced compression, which is the result of the decomposition of degradable solid particles.

Both primary compression and secondary compression are significantly affected by the composition and moisture content of MSW [17–20]. The composition and moisture content of fresh MSW produced in developing countries are significantly different to that of the waste produced in developed countries. The uppermost component of MSWs in developing countries such as China, India and Brazil, is food waste (fast-decomposed materials), which accounts for 40%–85% of the total wet weight [21,22]. However, MSWs in developed countries such as USA, UK and France have the highest content of paper and cardboard (slowly-decomposed materials), which accounts for 25%–66% of the total wet weight [21]. These two types of MSW can be named as high-food-waste-content (HFWC) MSW and low-food-waste-content (LFWC) MSW, respectively. The moisture content of fresh food waste is much higher than that of the other components of MSW, hence, the moisture content of HFWC-MSW is considerably higher than that of LFWC-MSW. For example, the moisture content of fresh MSW is 40%–60% in China, whereas it is 15%–40% for American MSW [21]. On the above accounts, the settlement behaviors between HFWC-MSW and LFWC-MSW landfills may be significantly different. Therefore, it is of great academic values to compare the settlement behaviors of these two types of MSWs, which is beneficial to a deep understanding of compression mechanism. However, few studies have been conducted to focus on this topic.

Many settlement models have been proposed for primary compression, mechanical creep and bio-induced compression of MSW. The most commonly used approach for estimating primary compression is similar to the one-dimensional primary consolidation theory of soils [1,23,24], and the method based on critical state soil mechanics which separates the primary compression into elastic and plastic components was also adopted in recent refs. [4,25]. The mechanical creep is often computed by the method similar to the one-dimensional secondary consolidation theory [1,2,23] and the rheological model that incorporates a compression parameter and a rate parameter [25,26]. The bio-induced compression is normally estimated via similar approaches as for mechanical creep [18], which is based on first-order reaction kinetics [2,11,25,27], or/and incorporates mass loss due to biodegradation [4]. Single mathematical functions are sometimes involved in some of the models to estimate the time-dependent secondary compression, such as the logarithmic model [10,28], the power model [29], the hyperbolic model [7], the equivalent-time-lines model [30] and the model based on first-order reaction kinetics [3]. Composite settlement models which combine different mathematical formulations from those described above have also been widely used to estimate both primary and secondary compressions of MSW [1–4,18,23–26,31].

Comparison of the currently available settlement models is essential so as to choose the most appropriate approach to estimate the settlement of different MSW landfills. Park et al. [28] applied five models to predict the settlement of nine landfill sites including both fresh MSW landfills (fill age < 5 years) and old MSW landfills (fill age > 20 years) in the USA and the UK. A considerable variation in the settlement of the fresh MSW landfills was obtained by using the different models, while limited variation was obtained for the old MSW landfills. Babu et al. [5] proposed a constitutive model and found that it predicted the total settlement of MSW to be in a range which was similar to the settlement predicted by the other reported models. Bareither and Kwak [32] conducted an evaluation of MSW settlement models based on two field-scale datasets from USA and concluded that the model presented by Gourc et al. [2] performed the best. However, these previous studies mainly focused on the settlement prediction for LFWC-MSW landfills, but not for HFWC-MSW landfills, which is extremely important for the design and management of landfill sites in developing countries. In addition, limited work has been done to focus on the comprehensive assessment of the settlement models from multiple aspects, e.g., computational simplicity, fitting performance, prediction performance and parametric stability.

In this paper, the settlement behaviors of HFWC-MSW and LFWC-MSW were characterized and compared based on the extensive datasets obtained from references. In addition, a methodology named the entropy method was built to select models for predicting the settlement at HFWC-MSW and LFWC-MSW landfills. The applicability of nine published MSW settlement models were evaluated based on the datasets obtained from four large-scale model tests. The four tests are (1) CARs from Ivanova et al. [15], (2) DTBE from Bareither et al. [33], (3) ZJU-CELL1 from Zhan et al. [21], and (4) ZJU-CELL2 from Xu [34]. The wastes in tests CARs and DTBE belong to LFWC-MSW, whereas in tests ZJU-CELL1 and ZJU-CELL2 are HFWC-MSWs.

2 Settlement behaviors of LFWC-MSW and HFWC-MSW

2.1 Primary compression ratio (C'_c)

Primary compression ratio (C'_c), which is the slope of the curve of the strain versus logarithmic effective stress, is commonly used to predict the primary compression of MSW. The C'_c values of fresh HFWC-MSW, fresh LFWC-MSW, aged HFWC-MSW and aged LFWC-MSW, are summarized in Figure 1 [3,13,16,17,21,22,34–54]. The average C'_c values of fresh HFWC-MSW and fresh LFWC-MSW are 0.33 and 0.22, respectively, while the average C'_c values of the aged

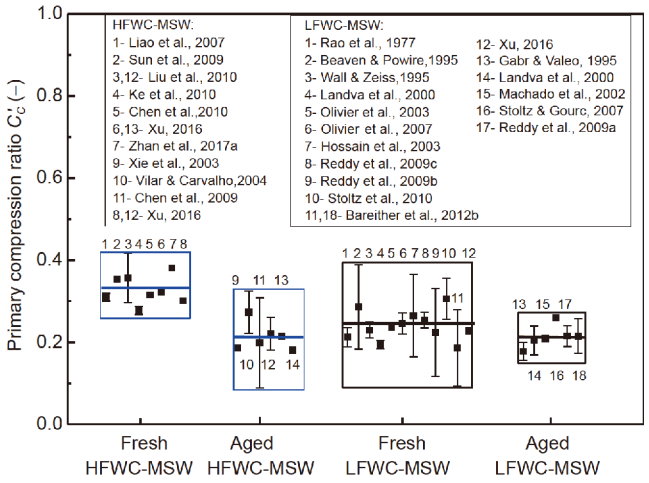

Figure 1 Summary of C'_c values for different types of MSWs [3,13,16,17,21,22,34–54].

HFWC-MSW and aged LFWC-MSW are both approximate 0.21. The larger average C'_c value of fresh HFWC-MSW, compared to that of the other types MSW, is mainly attributed to its higher food waste content [21]. Food waste contains plenty of intra-particle water within individual particles. The intra-particle water can be squeezed out from food waste that is subjected to an additional stress [55]. Therefore, food waste is more compressible than most of the other components of MSW, and the MSW with higher food waste content may result in a larger C'_c value.

2.2 Secondary compression process

Secondary compression strain plotted against time for LFWC-MSW and HFWC-MSW are summarized in Figure 2 [8,13–16,34,38,56–63]. The long-term secondary compression can be divided into three phases: (I) transitional phase; (II) active biodegradation phase; (III) residual phase [18,19,24]. To compare the behavior of secondary compression process, the slopes in the strain versus logarithmic time curves ($C'_{\alpha 1}$, $C'_{\alpha 2}$ and $C'_{\alpha 3}$) and the starting times of the three secondary compression phases (t_1, t_2 and t_3) are summarized in Figure 3. The starting time t_1 also implies the duration of the primary compression process.

During the transitional phase, Phase I, the $C'_{\alpha 1}$ values of HFWC-MSW are significantly greater than that of LFWC-MSW (Figure 3(a)), which indicates that the settlements of HFWC-MSW are significantly larger accordingly. In this phase, the biodegradation process of LFWC-MSW is retarded due to the high content of slowly-decomposed materials (i.e., paper), and therefore, the settlement is dominated by mechanical creep. HFWC-MSW has high content of fast-decomposed materials (i.e., food waste), resulting in a rapid development of hydrolysis process, and therefore, the settlement is not only due to creep, but also due to biodegradation induced compression. Because of the fact that the mechanical creep contributes significantly less to the total settlement compared to active biodegradation [64], the settlement of HFWC-MSW is much larger than LFWC-MSW. In addition, the values of the starting time (t_1) of HFWC-MSWs are in a similar range to that of LFWC-MSW (Figure 3(b)), which means that HFWC-MSW and LFWC-MSW have comparative duration of the primary compression process.

In the active biodegradation phase, Phase II, the slowly-decomposed materials continuously hydrolyze into dissolved compounds, and hence the settlement is mainly induced by biodegradation. It is observed from Figure 3(a) that the $C'_{\alpha 2}$ values of LFWC-MSW are much larger than that of HFWC-MSW. This can be explained by the fact that the content of slowly-decomposed materials is higher in LFWC-MSW than that in HFWC-MSW at dry mass basis [65]. It is observed from Figure 3(b) that the starting time (t_2) for HFWC-MSW is earlier than that for LFWC-MSW. This might be associated with the existence of robust microbial community inherited from the transitional phase for HFWC-MSW, which promoted the degradation process in active biodegradation phase. Furthermore, it should be noted that the

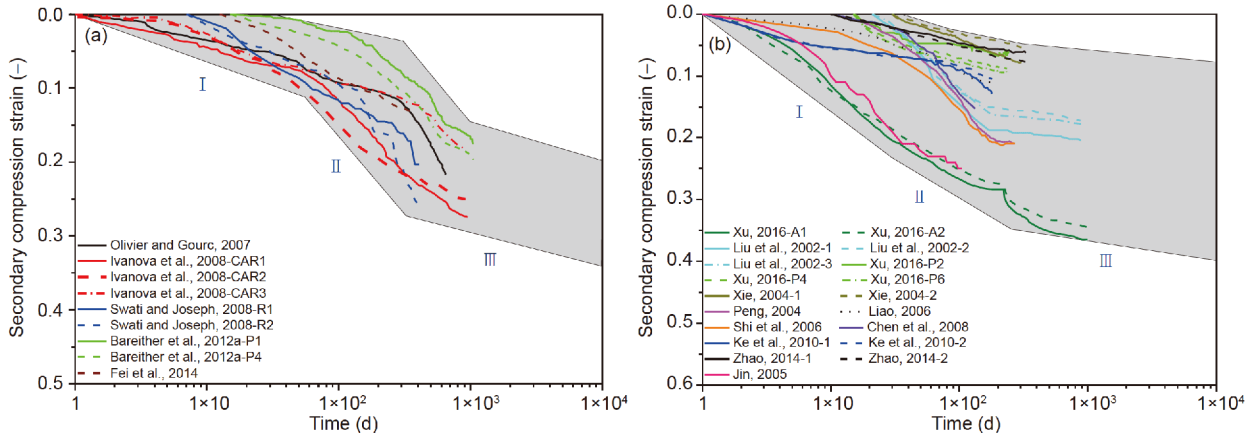

Figure 2 Secondary compression curves of (a) LFWC-MSW and (b) HFWC-MSW [8,13–16,34,38,56–63].

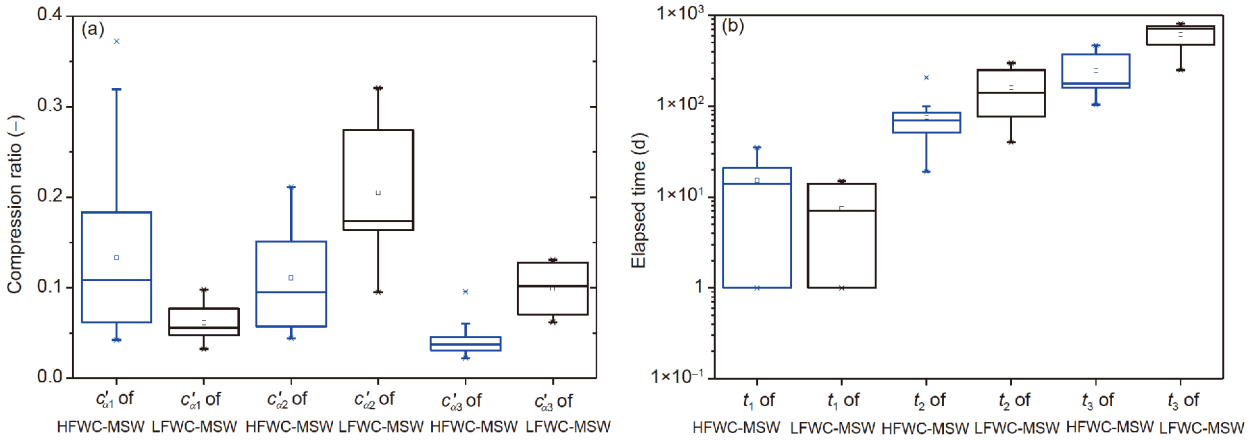

Figure 3 Box plots of (a) $C'_{\alpha1}$, $C'_{\alpha2}$ and $C'_{\alpha3}$ and (b) t_1, t_2 and t_3. The upper and lower lines of the box represent the 25th and 75th percentile of the data; the central line in the box represents the median value; the small square in the box represents the mean value; and the upper and lower whiskers extending from the box constitute 5th and 95th percentile of the data.

values of $C'_{\alpha2}$ are significantly larger than $C'_{\alpha1}$ for LFWC-MSW. However, for HFWC-MSW, the values of $C'_{\alpha2}$ are comparable to $C'_{\alpha1}$, and therefore it is normally difficult to separate these two phases in the strain-logarithmic time curves of HFWC-MSW.

In the residual phase, Phase III, the decomposition of the available degradable materials tends to come to an end, resulting in slowdown settlements. Subdued hydrolysis and creep are the two major contributors to the settlement in this phase [19]. This phase has received less attention because of the long time that elapses before it initiates, and therefore limited test data were reported in literature to support this transition, as shown in Figure 2. It is observed from Figure 3(a) that the average value of $C'_{\alpha3}$ for LFWC-MSW is much higher than that for HFWC-MSW. This might be associated with the higher content of residual organic matters contained in LFWC-MSW than that in HFWC-MSW at dry mass basis [66]. The starting time (t_3) for HFWC-MSW is much earlier than that for LFWC-MSW, which is because the active biodegradation phase for HFWC-MSW is shorter in duration due to the better degradation conditions and lower content of slowly-decomposed materials.

Based on the above analysis, the slopes of the strain versus logarithmic time curves in the three secondary compression phases can be characterized as "slight-steep-slight" for LFWC-MSW and "moderate-moderate-slight" for HFWC-MSW.

3 Settlement models

The performances of nine models in predicting the settlement of LFWC-MSW and HFWC-MSW were assessed in this paper. The general descriptions and the mathematical formulations of these models are summarized as below.

(1) Sowers model [1]

Sowers [1] found that the settlement of MSW was similar to that of peat and estimated the primary and secondary settlements of MSW by using the mathematical formulations of soil settlement model. Bjarngard and Edgers [23] proposed a settlement model which contains two phases of secondary compression. Following, Hossain and Gabr [24] introduced a third phase of secondary compression. As described in Sect. 2, the three phases are transitional phase, active biodegradation phase and residual phase. The mathematical formulation can be expressed as

$$S_T = S_P + S_S = H_0 C'_c \lg\left(\frac{\sigma_v + \Delta\sigma_v}{\sigma_{v0}}\right) + H_{EOP}\left[C'_{\alpha1}\lg\left(\frac{t}{t_1}\right) + C'_{\alpha2}\lg\left(\frac{t}{t_2}\right) + C'_{\alpha3}\lg\left(\frac{t}{t_3}\right)\right], \quad (1)$$

where S_T, S_P and S_S refer to the total settlement, the primary settlement and the secondary settlement, respectively, H_0 is the initial thickness of the waste layer prior to the primary settlement, H_{EOP} is the thickness of the waste layer at the end of the primary settlement (H_{EOP}= $H_0 S_P$), σ_v, σ_{v0} and $\Delta\sigma_v$ are the initial, the pre-consolidation and the additional vertical stresses at the middle of the waste layer, respectively.

(2) Logarithmic model [10]

Yen and Scanlon [10] proposed a logarithmic model to compute the time-dependent secondary settlement by assuming the settlement rate decreases linearly with the logarithmic median fill age of the waste, which is expressed as

$$S_S = \begin{cases} H_{EOP}\left(t - \frac{t_c}{2}\right)\left\{\alpha + \frac{\beta}{\ln 10}\left[\ln\left(t - \frac{t_c}{2}\right) - 1\right]\right\}, & t \le 10^{-\alpha/\beta} + \frac{t_c}{2}, \\ H_{EOP}\left(-\frac{\beta}{\ln(10)}10^{-\alpha/\beta}\right), & t > 10^{-\alpha/\beta} + \frac{t_c}{2}, \end{cases} \quad (2)$$

where t_c is the duration of waste placement, t is the elapsed

time since the beginning of waste placement, α and β are fitting parameters.

(3) Power model [29]

The power model proposed by Edil et al. [29] is a relationship for the time-dependent secondary settlement under a constant stress and is expressed as

$$S_S = H_{EOP}\Delta\sigma_v m\left(\frac{t}{t_r}\right)^n, \tag{3}$$

where m is the reference compressibility, n is the rate of compression, and t_r is the reference time introduced into the equation for time dimensionless (typically taken as 1 d).

(4) Hyperbolic model [7]

Ling et al. [7] used the following expression to compute the time-dependent secondary settlement of MSW landfills, which is similar to the hyperbolic function that has been used successfully in predicting the settlement of embankment on soft ground [67]

$$S_S = \frac{t}{1/\rho_0 + t/S_{S,ult}}, \tag{4}$$

where ρ_0 is the initial rate of settlement, $S_{S,ult}$ is the ultimate secondary settlement of MSW, $S_{S,ult} = H_{EOP}\times\varepsilon_{S,ult}$, $\varepsilon_{S,ult}$ is the ultimate secondary compression strain.

(5) Marques et al. (2003) model [26]

Marques et al. [26] developed a composite settlement model that explicitly took into account of primary compression, mechanical creep and bio-induced compression to calculate MSW landfill settlements, which is expresses as

$$S_T = H_0\left\{C'_c\lg\left(\frac{\sigma_v+\Delta\sigma_v}{\sigma_{v0}}\right) + b\Delta\sigma_v(1-e^{-ct}) + \varepsilon_{BIO}[1-e^{-k(t-t_2)}]\right\}, \tag{5}$$

where b is the coefficient of mechanical creep, c is the rate constant for mechanical creep, ε_{BIO} is the total amount of bio-induced compression strain, and k is the first-order rate constant for biodegradation.

(6) Machado et al. (2009) model [4]

Machado et al. [4] presented a composed settlement model to reproduce the time-dependent secondary settlement of MSW landfill, in which the mass loss related to methane generation is highlighted. This model can be expressed as

$$S_S = H_{EOP}C'_{\alpha 1}\lg\left(\frac{t}{t_1}\right) + H_{EOP}\frac{\rho_{s0}L_0}{\rho_{p0}C_m(1+e_0)}\left\{\left(1+\frac{\alpha^* L_0}{C_m}\right)[1-e^{-k(t-t_2)}] - \frac{\alpha^* L_0}{2C_m}[1-e^{-2k(t-t_2)}]\right\}, \tag{6}$$

where ρ_{s0} is the initial density of MSW solid materials, ρ_{p0} is the initial density of MSW paste (non-fibrous material), L_0 is the methane generation potential of MSW(dry mass basis), C_m is the methane generation potential of organic matter contained in MSW (dry mass basis), e_0 is the initial void ratio, α^* is a degradation rate parameter.

(7) Gourc et al. (2010) model [2]

Gourc et al. [2] developed a biomechanical model which combines mechanical creep and bio-induced compression based on the first-order reaction kinetics to predict the secondary settlement of MSW. The model is expressed as

$$S_S = H_{EOP}\left\{C'_{\alpha 1}\lg\left(\frac{t}{t_1}\right) + \varepsilon_{BIO}[1-e^{-k(t-t_2)}]\right\}. \tag{7}$$

(8) Chen et al. (2010) model [3]

Chen et al. [3] presented the following composite settlement model that combines mechanical creep and bio-induced compression into a single mathematical formulation based on first-order kinetics

$$S_T = H_0C'_c\lg\left(\frac{\sigma_v+\Delta\sigma_v}{\sigma_{v0}}\right) + H_{EOP}\varepsilon_{S,ult}[1-e^{-c_t(t-t_1)}], \tag{8}$$

where c_t is the first-order rate constant for coupled mechanical creep and bio-induced compression.

(9) Gao et al. (2017) model [30]

Based on the time-lines model for clays, Gao et al. [30] developed an equivalent-time-lines model for the settlement prediction of MSW under both normal and enhanced biodegradation conditions, which is expressed as

$$S_T = H_0\left\{C'_c\lg\left(\frac{\sigma_v+\Delta\sigma_v}{\sigma_{v0}}\right) + \varepsilon_{MB}{}^*(\sigma_v+\Delta\sigma_v)(1-e^{-c_t(t-t_1)})\right\}, \tag{9}$$

$$\varepsilon_{MB}{}^*(\sigma_v+\Delta\sigma_v) = \begin{cases} \varepsilon_{MB}{}^*(\sigma_r) + (C'_{c\infty}-C'_{c0})\lg\left(\dfrac{\sigma_v+\Delta\sigma_v}{\sigma_r}\right), & \sigma_v+\Delta\sigma_v \le \sigma_r\times 10^{\varepsilon_{MB}{}^*(\sigma_r)/(C'_{c0}-C'_{c\infty})}, \\ 0, & \sigma_v+\Delta\sigma_v > \sigma_r\times 10^{\varepsilon_{MB}{}^*(\sigma_r)/(C'_{c0}-C'_{c\infty})}, \end{cases} \tag{10}$$

where σ_r is a reference vertical stress, $\varepsilon_{MB}{}^*(\sigma)$ is the ultimate strain (on the basis of H_0) due to mechanical creep and bio-induced compression under σ, C'_{c0} is the primary compression index of the fresh MSW and $C'_{c\infty}$ is the primary compression index of completely biodegraded MSW.

In the following analysis, when computing the total settlement of MSW, the primary settlement term in eq. (1) was incorporated into the time-dependent models, i.e., eqs. (2), (3), (4), (6) and (7).

4 Assessment of settlement models by using entropy method

4.1 Entropy method

To evaluate the comprehensive performance of each settle-

ment model, four criterions were considered: (1) computational simplicity (N), (2) fitting performance (R^2), (3) prediction performance (ε_{ex}), and (4) parametric stability (RMSE, i.e., root mean square error of the compression strain). A good settlement model should contain as few parameters as possible to yield a simple computation process and a high statistic performance. The parameters can be classified into four categories: measured, fixed, computed and optimized [32]. The optimized parameters are obtained via least squares analysis based on the existing settlement data. Large number of optimized parameters increases the uncertainty of the calculated results. In addition, a good model also requires satisfied fitting and prediction performance. The fitting performance is evaluated by computing the determination coefficient of least squares optimization based on the measured data, and the prediction performance is assessed based on the anticipated long-term settlement beyond the range of the measured data. Moreover, a good model is also expected to be stable in the optimized parameters when waste properties and experimental conditions are similar. The parametric stability is assessed by the simulation performance by using RMSE of compression strain, which is computed as

$$\text{RMSE}=\sqrt{\frac{1}{M}\sum_{s=1}^{M}(R_s-\overline{R}_s)^2}, \tag{11}$$

where M is the total number of measured data for a certain MSW sample, R_s is the measured compression strain and $\overline{R}_s$ is the modeled compression strain using the average value of optimized parameters from cases under similar conditions.

The entropy method is a weighting determination method based on the dispersion degree of the criterion value. The influence of a criterion on the comprehensive evaluation is considered to be positively related to its dispersion degree, which can be determined by entropy value. The implementation of entropy method in this study includes the following steps.

First, an information matrix ($\mathbf{X}_{9\times4}$) is established

$$\mathbf{X}_{9\times4}=\begin{matrix}\\ \text{Models}\end{matrix}\begin{matrix}\overset{\text{Indicators}}{\overbrace{}}\\ \begin{bmatrix}x_{11} & \cdots & x_{14}\\ \cdots & \cdots & \cdots\\ x_{91} & \cdots & x_{94}\end{bmatrix}\end{matrix}, \tag{12}$$

where indicators refer to the average value of the four criterions, i.e., (1) $\overline{N}$, (2) $\overline{R^2}$, (3) $\overline{\varepsilon_{ex}}$ and (4) $\overline{\text{RMSE}}$; x_{ij} is the magnitude of indicator j with respect to model i.

Then, the nine values in each column vector of the matrix ($\mathbf{X}_{9\times4}$) were normalized and a normalized information matrix ($\mathbf{R}_{9\times4}$) is obtained.

$$\begin{matrix}\\ \text{Models}\end{matrix}\begin{matrix}\overset{\text{Indicators}}{\overbrace{}}\\ \begin{bmatrix}x_{11} & \cdots & x_{14}\\ \cdots & \cdots & \cdots\\ x_{91} & \cdots & x_{94}\end{bmatrix}\end{matrix}\xrightarrow{\text{normalize}}\begin{matrix}\\ \text{Models}\end{matrix}\begin{matrix}\overset{\text{Indicators}}{\overbrace{}}\\ \begin{bmatrix}r_{11} & \cdots & r_{14}\\ \cdots & \cdots & \cdots\\ r_{91} & \cdots & r_{94}\end{bmatrix}\end{matrix}, \tag{13}$$

where r_{ij} is the normalized value of x_{ij} and can be presented as follows:

$$r_{ij}=\begin{cases}\dfrac{x_{ij}^{\max}-x_{ij}}{x_{ij}^{\max}-x_{ij}^{\min}},\ j=1,4,\\ \dfrac{x_{ij}-x_{ij}^{\min}}{x_{ij}^{\max}-x_{ij}^{\min}},\ j=2,\\ 1-\dfrac{\left|x_{ij}-x_{*j}\right|}{\left|x_{ij}-x_{*j}\right|_{\max}},\ j=3,\end{cases} \tag{14}$$

where $x_{ij}^{\max}$ and $x_{ij}^{\min}$ are maximum and minimum values of all x_{ij}, respectively, and x_{*j} is the reference value of indicator j.

Next, the entropy value (H_j) of indicator j , i.e., the element of entropy vector (**H**), is calculated by

$$\begin{aligned}&H_j=-\frac{1}{\ln(9)}\sum_{i=1}^{9}f_{ij}\times\ln(f_{ij}),\\ &\textbf{s.t.}\ IF\ f_{ij}=0,\ f_{ij}\times\ln(f_{ij})=0,\end{aligned} \tag{15}$$

where f_{ij} is the weight of r_{ij} and can be determined as

$$f_{ij}=\frac{r_{ij}}{\sum_{i=1}^{9}r_{ij}}. \tag{16}$$

Finally, the weight of each indicator (w_j), i.e., the element of weight vector (**W**), can be computed as

$$w_j=\frac{1-H_j}{4-\sum_{j=1}^{4}H_j}. \tag{17}$$

4.2 Comprehensive scores for the settlement models

The number of independent parameters in model i (i=1–9) can be scored as

$$(S_1^*)_i=\frac{N_i^{\min}}{N_i}, \tag{18}$$

where N_i is the total number of parameters in model i, $N_i^{\min}$ is the minimum value of all N_i.

The fitting performance of each model can be scored as

$$(S_2^*)_i=\frac{(\overline{R^2})_i}{(\overline{R^2})_i^{\max}}, \tag{19}$$

where $(\overline{R^2})_i$ is the average determination coefficient of model i, $(\overline{R^2})_i^{\max}$ is the maximum value of all $(\overline{R^2})_i$.

The prediction performance of each model can be scored as

$$(S_3^*)_i=\frac{1}{M}\sum_{k=1}^{M}(S_3^*)_{ki}=\frac{1}{M}\sum_{k=1}^{M}\left(1-\frac{\left|\varepsilon_{ex,ki}-\varepsilon_{ex,k*}\right|}{\varepsilon_{ex,k*}}\right), \tag{20}$$

where M is the number of predictions, $(S_3^*)_{ki}$ is a sub-score of

model i for prediction k; $\varepsilon_{ex,ki}$ is the extrapolated long-term strain applying model i for prediction k; $\varepsilon_{ex,k*}$ is the reference extrapolated long-term strain. If $(S_3^*)_{ki}$ is negative, it is valued as zero in this analysis.

The stability of optimized parameters in model i can be scored as

$$(S_4^*)_i = \frac{(\overline{\mathrm{RMSE}})_i^{\min}}{(\overline{\mathrm{RMSE}})_i}, \tag{21}$$

where $(\overline{\mathrm{RMSE}})_i$ is the average value of root mean square error of the compression strain for settlement model i by using average values of optimized parameters; $(\overline{\mathrm{RMSE}})_i^{\min}$ is the minimum value of all $(\overline{\mathrm{RMSE}})_i$.

Finally, the comprehensive score (S_i^*) of settlement model i can be computed as

$$S_i^* = \sum_{j=1}^{4} w_j \times (S_j^*)_i. \tag{22}$$

5 Assessment of settlement models for LFWC-MSW

5.1 Large-scale compression tests of LFWC-MSW from references

Ivanova et al. [15] conducted long-term compression tests on LFWC-MSW by using two consolidating anaerobic reactors (CARs), which comprised a perspex cylinder to hold the waste and a loading system to apply a constant stress to the waste. The perspex cylinder had an internal diameter of 0.48 m and an approximate height of 0.90 m. The main components of the MSW specimen were paper, plastic and yard waste, accounting for 27.3%, 20.0% and 18.4% respectively on dry mass basis. Samples of the waste were loosely placed into each reactor and then compressed by self-weight until the height of waste reached approximately 0.80 m. The initial vertical stresses (σ_v) and the pre-consolidation stresses (σ_{v0}) at the middle of the waste layer were considered to be the same, and were 1.2654 kPa and 1.3819 kPa for CAR1 and CAR2, respectively. After the self-weight compression of the wastes, additional vertical stresses ($\Delta\sigma_v$) of 150 kPa and 50 kPa were then applied to CAR1 and CAR2, respectively. The compression strain was measured every 24 h over a duration of 919 d, and the results are shown in Figure 4(a). Secondary compression was considered to start on Day 2 (i.e. t_1 = 1 d) and the height of waste layer at the end of the primary compression (H_{EOP}) was 0.34 m for CAR1 and 0.42 m for CAR2. The starting time t_2 were 55 d and 32 d for CAR1 and CAR2, respectively.

Another experimental study on LFWC-MSW settlement was carried out by Bareither [33], which is called the Deer Track Bioreactor Experiment (DTBE). The experiment was conducted in a lysimeter with a height of 8.2 m and a diameter of 2.4 m. The main components of the waste were paper and plastic, being 24.6% (16.1%) and 8.4% (9.5%) of the total amount of the wet (dry) waste. The whole waste column was divided into four layers from the bottom to the top, L1, L2, L3 and L4, with the initial thickness of 1.80, 2.23, 2.00 and 1.76 m, and the initial unit weight of 9.16, 6.29, 6.62 and 7.42 kN/m^3, respectively. The σ_v (or σ_{v0}) at the middle of L1, L2, L3 and L4, were calculated as 8.26, 7.03, 6.63 and 6.50 kPa, respectively. Approximately a thickness of 0.9 m of gravel was placed at the top of the waste column for leachate recirculation, corresponding to an additional stress ($\Delta\sigma_v$) of 19.5 kPa. Four settlement plates were placed at the top of each waste layer to measure the daily settlement for 1049 d. Apart from layer L4 where bio-induced compression was not observed, complete settlement behaviors were observed in the other layers L1, L2 and L3. Therefore, L4 was not included in the following analysis. The developments of compression strain for each waste layer are shown in Figure 4(b). t_1 was determined as 15 d by using the first-order rate equation presented in Handy [68], and t_2 was determined as 164 d via leachate *COD* (chemical oxygen

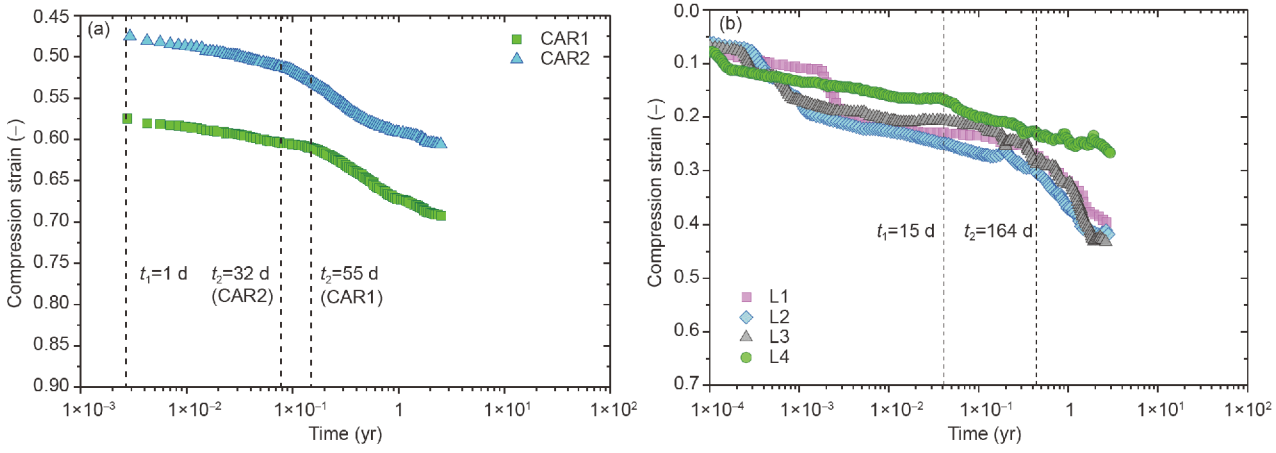

Figure 4 Cumulative compression strain versus time for (a) CARs and (b) DTBE.

demand) analysis.

5.2 Fitting, prediction and simulation of LFWC-MSW settlement

The compression strain of LFWC-MSW were fitted and predicted by using the nine settlement models as described in Sect. 3, based on the settlement data from CARs and DTBE, as shown in Figure 5. All models yielded good fitting performance (R^2 >0.93), indicating that they have the ability to capture the settlement behavior of LFWC-MSW under different stresses and degradation conditions. However, the models exhibited different performances for the predicted results of the settlement beyond the range of the measured data. The predicted settlement turned to increase sharply and continuously at certain elapsed times for the power model, which was considered to be impractical. The settlement in residual phase computed by the models proposed by Machado et al. [4], Gourc et al. [2] and Sowers et al. [1] continued to increase in a slow rate, while by the logarithmic model, the hyperbolic model and the models proposed by Marques et al. [26], Chen et al. [3] and Gao et al. [30] tended to be constrained to a limit value. These two trends are considered to be reasonable according to the secondary settlement behavior of LFWC-MSW.

The settlement data from CARs and DTBE were simulated by the nine settlement models by using the average value of optimized parameters, and the results are shown in Figure 6. The simulated primary compression strain was well fitted into the measured data of CAR1 and the two layers, L2 and L3 of DTBE, but slightly overestimated for CAR2 and slightly underestimated for L1 of DTBE. The simulation performance of primary compression is mainly dominated by the variation of C'_c which was obtained from the five cases, therefore, the smaller standard deviation (*SD*) of C'_c, the better simulation effect. On the whole, the primary compression was satisfactorily simulated due to the minor variation of C'_c (*SD*=0.02). The large difference between simulated secondary compression and measured data was observed for the power model, Marques et al. [26] and Machado et al. [4]. The secondary compression predicted by the power model was proved to be impractical judging from the general shapes of its predicting curves. The general shape of the secondary settlement simulated by Marques et al. [26] was significantly deviated from the measured data of CARs. This was mainly attributed to that the parameter b in this model has stress-dependent behavior [32], a probable decreasing trend for b with respect to $\Delta\sigma_v$ can be observed from Table 1. Therefore, when applying the model proposed by Marques et al. [26], the relationships between b and $\Delta\sigma_v$ need to be set up. The secondary settlement simulated by the model proposed by Machado et al. [4] was highly overestimated beyond a time point for the CARs, however, the model demonstrated fairly satisfactory results for the DTBE. This was primarily attributed to the average values of bio-induced compression parameters (α^* and k) were comparable to that obtained from the DTBE and were much larger than that from the CARs. Therefore, when applying the model proposed by Machado et al. [4], the parameters related to bio-induced compression should be determined specifically according to the actual conditions of the landfill. Overall, the model proposed by Gourc et al. [2] yielded relatively higher statistical performances when using average value of optimized parameters.

5.3 Recommendation of settlement model for LFWC-MSW

Based on the entropy method described in Sect. 4.1, the average value of each factor corresponding to each settlement model is listed in matrix **X** in Table 2. After adding the primary compression component into the secondary compression models, the empirical models (logarithmic, power and hyperbolic) and the model proposed by Chen et al. [3] have the lowest number of independent optimized parameter ($\overline{N}$ = 3), while Machado et al. [4] has the highest ($\overline{N}$ = 5). All the nine models had perfect fitting performance for CARs and DTBE datasets ($\overline{R^2} > 0.97$), and therein Sowers et al. [1], Gourc et al. [2] and Marques et al. [26] performed the best ($\overline{R^2} > 0.99$). The average long-term settlement strains ($\overline{\varepsilon_{ex}}$) extrapolated to 100 years by all models were in the range of 0.5435–0.6673, except for the power model ($\overline{\varepsilon_{ex}}$ = 1). The extrapolations provided by Sowers et al. [1] were considered to be reference values (ε_{ex,k^*}), since its shapes of calculated strain-time curves can well depict the compression behavior of LFWC-MSW. When using the average value of optimized parameters, Gourc et al. [2], Sowers et al. [1] and hyperbolic model exhibited good simulation performance ($\overline{\text{RMSE}} < 0.03$).

The entropy-based weight of $\overline{N}$, $\overline{R^2}$, $\overline{\varepsilon_{ex}}$ and $\overline{\text{RMSE}}$ were obtained as 0.1973, 0.4590, 0.1374 and 0.2063, respectively, as shown in Table 2. These values were utilized to calculate comprehensive score for each settlement model, the results are presented in Table 3. It shows that the models proposed by Gourc et al. [2] and Sowers et al. [1] achieved the highest comprehensive score, which are 0.9461 and 0.9238, respectively. This suggests that these two models performed the best among all the nine settlement models. Therefore, the Gourc et al. [2] model and the Sowers et al. [1] model are recommended to predict the settlement at LFWC-MSW landfills.

The parameters in the models proposed by Gourc et al. [2] and Sowers et al. [1] can be obtained or estimated in the following ways. t_1 and S_p can be determined by using FORE method based on the measured data. Subsequently, C'_c can be

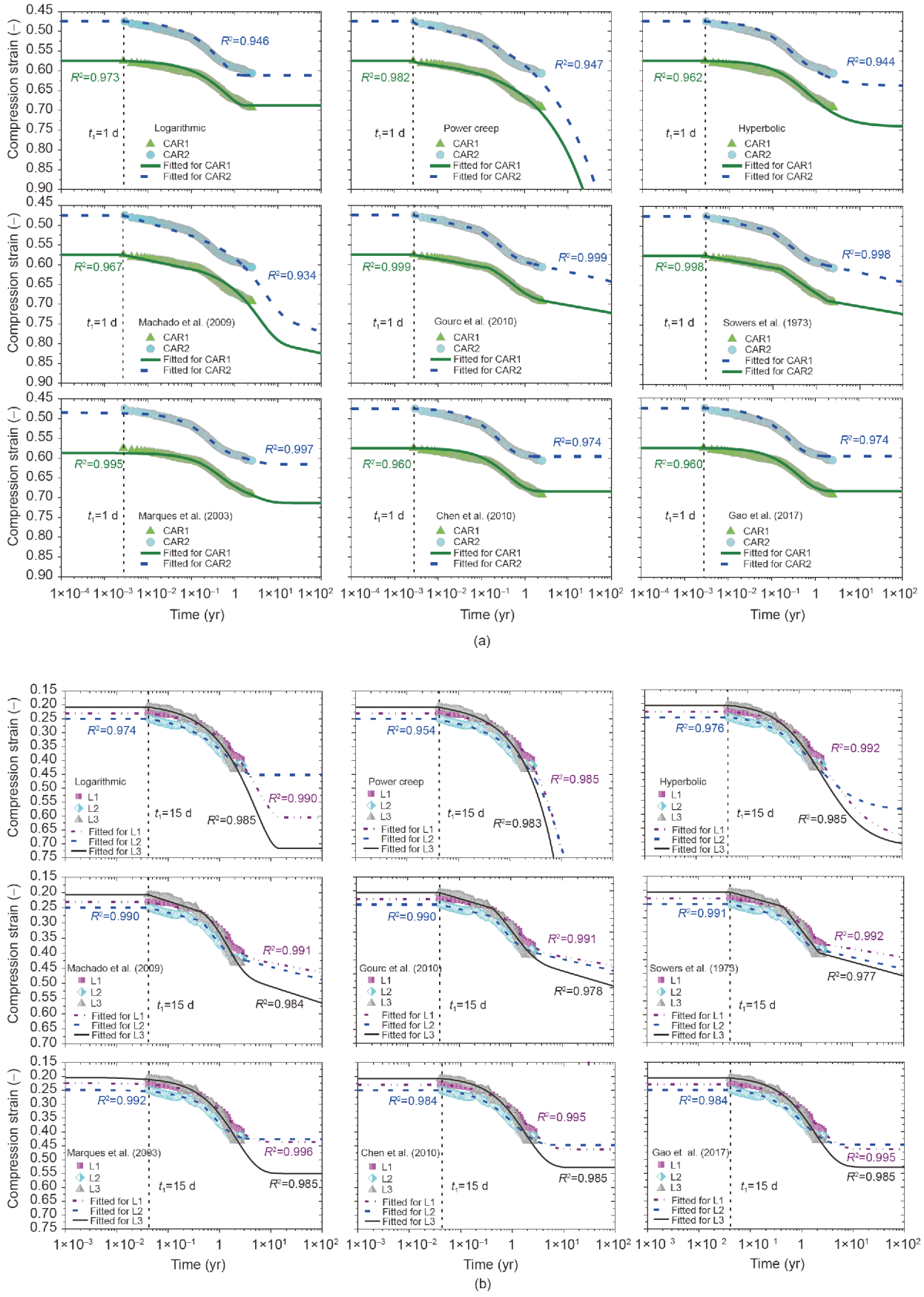

Figure 5 Fitted and predicted compression strains for (a) CARs and (b) DTBE.

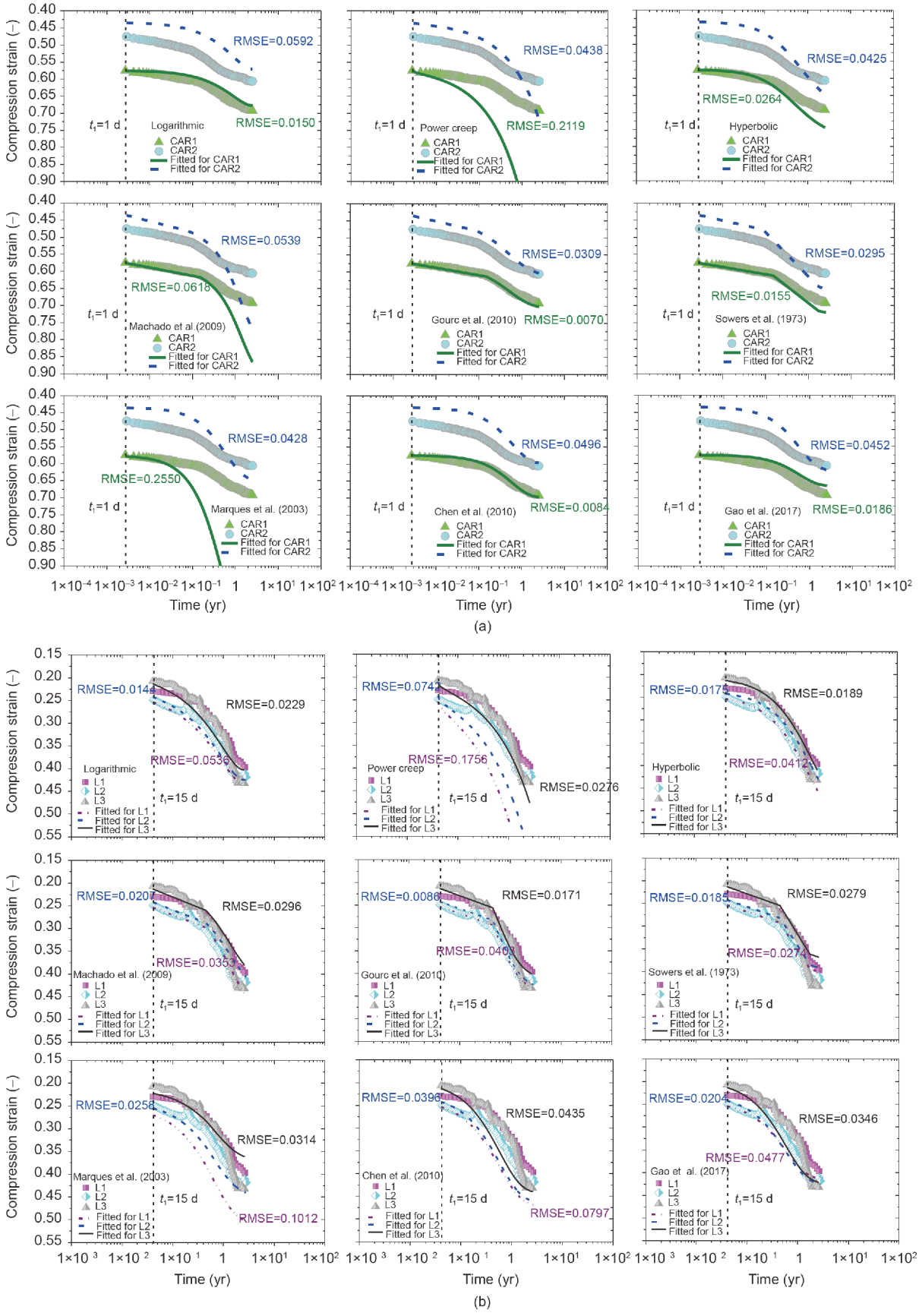

Figure 6 Simulated compression strains by using average value of optimized parameters for (a) CARs and (b) DTBE.

Table 1 Summary of model parameters for CARs, DTBE and ZJU-CELLs

Model	Para.	Unit	LFWC-MSW					Average	HFWC-MSW						Average
			CARs		DTBE				ZJU-CELL1			ZJU-CELL2			
			CAR1	CAR2	L1	L2	L3		L1	L2	L3	L1	L2	L3	
Logarithmic model [10]	σ_{v0}	kPa	1.27	1.38	8.26	7.03	6.63	–	3.43	8.44	9.30	3.72	8.92	10.13	–
	σ_v	kPa	1.27	1.38	8.26	7.03	6.63	–	3.43	8.44	9.30	3.72	8.92	10.13	–
	$\Delta\sigma$	kPa	150.00	50.00	59.82	45.76	32.50	–	67.67	50.79	32.20	77.31	59.47	39.20	–
	H_0	m	0.80	0.80	1.80	2.23	2.00	–	0.93	2.23	2.30	1.20	2.74	2.79	–
	C'_c	–	0.2768	0.3025	0.2511	0.2855	0.2685	0.2769	0.3978	0.3523	0.3567	0.3638	0.3745	0.3933	0.3731
	α	–	0.0840	0.0585	0.0872	0.0903	0.1205	0.0881	0	0	0	0	0	0	0
	β	–	–0.3524	–0.4426	–0.0737	–0.1397	–0.1049	–0.2227	–0.3309	–0.2367	–0.2503	–0.2814	–0.3979	–0.3788	–0.3127
	R^2	–	0.9728	0.9464	0.9899	0.9742	0.9852	–	0.7474	0.4321	–0.5221	0.6526	0.4844	–0.0066	–
Power creep model [29]	σ_{v0}	kPa	1.27	1.38	8.26	7.03	6.63	–	3.43	8.44	9.30	3.72	8.92	10.13	–
	σ_v	kPa	1.27	1.38	8.26	7.03	6.63	–	3.43	8.44	9.30	3.72	8.92	10.13	–
	$\Delta\sigma$	kPa	150.00	50.00	59.82	45.76	32.50	–	67.67	50.79	32.20	77.31	59.47	39.20	–
	H_0	m	0.80	0.80	1.80	2.23	2.00	–	0.93	2.23	2.30	1.20	2.74	2.79	–
	C'_c	–	0.2768	0.3025	0.2511	0.2855	0.2685	0.2769	0.3978	0.3523	0.3567	0.3638	0.3745	0.3933	0.3731
	m	kPa^{-1}	1.25×10^{-4}	5.35×10^{-4}	2.35×10^{-5}	7.44×10^{-5}	6.55×10^{-5}	2.00×10^{-4}	2.40×10^{-4}	3.38×10^{-4}	8.60×10^{-4}	2.33×10^{-4}	5.31×10^{-4}	9.76×10^{-4}	5.30×10^{-4}
	n	–	0.4117	0.3500	0.7482	0.6335	0.7351	0.5757	0.3722	0.2889	0.1983	0.3240	0.2804	0.2313	0.2825
	R^2	–	0.9819	0.9470	0.9855	0.9538	0.9835	–	0.8956	0.8903	0.7611	0.9139	0.9745	0.9453	–
Hyperbolic model [7]	σ_{v0}	kPa	1.27	1.38	8.26	7.03	6.63	–	3.43	8.44	9.30	3.72	8.92	10.13	–
	σ_v	kPa	1.27	1.38	8.26	7.03	6.63	–	3.43	8.44	9.30	3.72	8.92	10.13	–
	$\Delta\sigma$	kPa	150.00	50.00	59.82	45.76	32.50	–	67.67	50.79	32.20	77.31	59.47	39.20	–
	H_0	m	0.80	0.80	1.80	2.23	2.00	–	0.93	2.23	2.30	1.20	2.74	2.79	–
	C'_c	–	0.2768	0.3025	0.2511	0.2855	0.2685	0.2769	0.3978	0.3523	0.3567	0.3638	0.3745	0.3933	0.3731
	ρ_0	m/yr	0.2020	0.4345	0.2047	0.3816	0.3636	0.3173	0.6049	2.3798	5.4140	0.7989	4.0763	6.2162	3.2484
	$\varepsilon_{S,ult}$	–	0.3910	0.3101	0.5980	0.4501	0.6455	0.4789	0.1239	0.0791	0.0764	0.1106	0.1502	0.1347	0.1125
	R^2	–	0.9440	0.9622	0.9924	0.9759	0.9849	–	0.9288	0.9456	0.9017	0.8914	0.9703	0.9771	–
Machado et al. (2009) [4]	σ_{v0}	kPa	1.27	1.38	8.26	7.03	6.63	–	3.43	8.44	9.30	3.72	8.92	10.13	–
	σ_v	kPa	1.27	1.38	8.26	7.03	6.63	–	3.43	8.44	9.30	3.72	8.92	10.13	–
	$\Delta\sigma$	kPa	150.00	50.00	59.82	45.76	32.50	–	67.67	50.79	32.20	77.31	59.47	39.20	–
	H_0	m	0.80	0.80	1.80	2.23	2.00	–	0.93	2.23	2.30	1.20	2.74	2.79	–
	t_1	yr	0.0027	0.0027	0.0411	0.0411	0.0411	–	0.0795	0.0740	0.0685	0.0493	0.0384	0.0329	–
	t_2	yr	0.1507	0.0877	0.4493	0.4493	0.4493	–	0.1041	0.0986	0.0982	0.1452	0.1425	0.1370	–
	e_0	–	0.69	1.07	0.91	1.64	1.62	–	5.38	5.38	5.38	3.75	3.75	3.75	–
	ρ_{s0}	Mg/m^3	1.35	1.35	1.34	1.34	1.34	–	1.26	1.26	1.26	1.25	1.25	1.25	–
	ρ_{p0}	Mg/m^3	1.36	1.36	1.40	1.40	1.40	–	1.28	1.28	1.28	1.22	1.22	1.22	–
	L_0	m^3/Mg	247.8	247.8	118.3	118.3	118.3	–	268.6	268.6	268.6	274.1	274.1	274.1	–
	C_m	Mg/m^3	432.5	432.5	453.3	453.3	453.3	–	481.3	481.3	481.3	491.3	491.3	491.3	–
	C'_c	–	0.2768	0.3025	0.2511	0.2855	0.2685	0.2769	0.3978	0.3513	0.3567	0.3638	0.3745	0.3933	0.3729
	$C'_{\alpha1}$	–	0.0547	0.0628	0.0421	0.0563	0.0693	0.0570	0.1399	0.0967	0.0987	0.0967	0.1241	0.1118	0.1113
	α^*	–	0.0000	0.0000	1.8079	2.5418	9.7254	2.8150	–	–	–	–	–	–	–
	k	yr^{-1}	0.2682	0.1961	1.0128	2.1901	1.0048	0.9344	0	0	0	0	0	0	0
	R^2	–	0.9671	0.9344	0.9912	0.9904	0.9835	–	0.7813	0.5209	–0.2989	0.7845	0.7731	0.5400	–

(*To be continued on the next page*)

(*Continued*)

Model	Para.	Unit	LFWC-MSW						HFWC-MSW						
			CARs		DTBE			Average	ZJU-CELL1			ZJU-CELL2			Average
			CAR1	CAR2	L1	L2	L3		L1	L2	L3	L1	L2	L3	
Gourc et al. (2010) [2]	σ_{v0}	kPa	1.27	1.38	8.26	7.03	6.63	–	3.43	8.44	9.30	3.72	8.92	10.13	–
	σ_v	kPa	1.27	1.38	8.26	7.03	6.63	–	3.43	8.44	9.30	3.72	8.92	10.13	–
	$\Delta\sigma$	kPa	150.00	50.00	59.82	45.76	32.50	–	67.67	50.79	32.20	77.31	59.47	39.20	–
	H_0	m	0.80	0.80	1.80	2.23	2.00	–	0.93	2.23	2.30	1.20	2.74	2.79	–
	t_1	yr	0.0027	0.0027	0.0411	0.0411	0.0411	–	0.0795	0.0740	0.0685	0.0493	0.0384	0.0329	–
	t_2	yr	0.1507	0.0877	0.4493	0.4493	0.4493	–	0.1041	0.0986	0.0982	0.1452	0.1425	0.1370	–
	C'_c	–	0.2768	0.3025	0.2511	0.2855	0.2685	0.2769	0.3978	0.3513	0.3567	0.3638	0.3745	0.3933	0.3729
	$C'_{\alpha 1}$	–	0.0457	0.0466	0.0417	0.0556	0.0693	0.0518	0.1399	0.0967	0.0987	0.0967	0.1241	0.1118	0.1113
	k	yr^{-1}	1.9223	4.0358	0.8339	1.8428	0.8706	1.9011	–	–	–	–	–	–	–
	ε_{BIO}	–	0.1382	0.1072	0.1703	0.1294	0.1900	0.1470	0	0	0	0	0	0	0
	R^2	–	0.9988	0.9988	0.9913	0.9904	0.9780	–	0.7813	0.5209	–0.2989	0.7845	0.7731	0.5400	–
Sowers et al. (1973) [1]	σ_{v0}	kPa	1.27	1.38	8.26	7.03	6.63	–	3.43	8.44	9.30	3.72	8.92	10.13	–
	σ_v	kPa	1.27	1.38	8.26	7.03	6.63	–	3.43	8.44	9.30	3.72	8.92	10.13	–
	$\Delta\sigma$	kPa	150.00	50.00	59.82	45.76	32.50	–	67.67	50.79	32.20	77.31	59.47	39.20	–
	H_0	m	0.80	0.80	1.80	2.23	2.00	–	0.93	2.23	2.30	1.20	2.74	2.79	–
	t_1	yr	0.0027	0.0027	0.0411	0.0411	0.0411	–	0.0795	0.0740	0.0685	0.0493	0.0384	0.0329	–
	t_2	yr	0.1507	0.0877	0.4493	0.4493	0.4493	–	0.1041	0.0986	0.0982	0.1452	0.1425	0.1370	–
	t_3	yr	1.7843	0.7337	2.3934	1.5629	2.2472	1.7443	0.1420	0.1420	0.1420	0.5562	0.7659	0.8384	0.4311
	C'_c	–	0.2768	0.3025	0.2511	0.2855	0.2685	0.2769	0.3978	0.3513	0.3567	0.3638	0.3745	0.3933	0.3729
	$C'_{\alpha 1}$	–	0.0452	0.0462	0.0396	0.0569	0.0636	0.0503	0.2400	0.1864	0.2625	0.1304	0.1657	0.1610	0.1910
	$C'_{\alpha 2}$	–	0.1757	0.1614	0.2351	0.2796	0.3013	0.2306	0.2000	0.1673	0.1312	0.0605	0.0688	0.0454	0.1122
	$C'_{\alpha 3}$	–	0.0452	0.0462	0.0396	0.0569	0.0636	0.0503	0.0813	0.0401	0.0186	0.0400	0.0623	0.0683	0.0517
	R^2	–	0.9976	0.9981	0.9916	0.9914	0.9770	–	0.9148	0.9598	0.9275	0.9167	0.9619	0.9582	–
Marques et al. (2003) [26]	σ_{v0}	kPa	1.27	1.38	8.26	7.03	6.63	–	3.43	8.44	9.30	3.72	8.92	10.13	–
	σ_v	kPa	1.27	1.38	8.26	7.03	6.63	–	3.43	8.44	9.30	3.72	8.92	10.13	–
	$\Delta\sigma$	kPa	150.00	50.00	59.82	45.76	32.50	–	67.67	50.79	32.20	77.31	59.47	39.20	–
	H_0	m	0.80	0.80	1.80	2.23	2.00	–	0.93	2.23	2.30	1.20	2.74	2.79	–
	t_2	yr	0.1507	0.0877	0.4493	0.4493	0.4493	–	0.1041	0.0986	0.0982	0.1452	0.1425	0.1370	–
	b	kPa^{-1}	5.08×10^{-4}	1.89×10^{-3}	2.95×10^{-3}	2.33×10^{-3}	1.06×10^{-2}	3.70×10^{-3}	8.40×10^{-4}	1.87×10^{-3}	3.92×10^{-3}	8.07×10^{-4}	1.06×10^{-3}	2.01×10^{-3}	1.7×10^{-3}
	c	yr^{-1}	2.5456	4.2914	0.6758	1.4446	0.4785	1.8872	25.0146	32.9739	33.7290	36.9044	28.4845	30.3914	31.2496
	k	yr^{-1}	0.3885	0.5061	0.7064	1.4765	0.0010	0.6157	4.2937	1.8623	0.7725	1.3920	4.0555	2.9080	2.5473
	C'_c	–	0.2824	0.3091	0.2450	0.2836	0.2654	0.2771	0.3743	0.2811	0.2375	0.3409	0.3717	0.3809	0.3311
	ε_{BIO}	–	0.0503	0.0361	0.0354	0.0707	0.0010	0.0387	0.0280	0.0299	0.0245	0.0419	0.0366	0.0315	0.0321
	R^2	–	0.9949	0.9971	0.9960	0.9923	0.9852	–	0.9314	0.9854	0.9242	0.9399	0.9934	0.9943	–
Chen et al. (2010) [3]	σ_{v0}	kPa	1.27	1.38	8.26	7.03	6.63	–	3.43	8.44	9.30	3.72	8.92	10.13	–
	σ_v	kPa	1.27	1.38	8.26	7.03	6.63	–	3.43	8.44	9.30	3.72	8.92	10.13	–
	$\Delta\sigma$	kPa	150.00	50.00	59.82	45.76	32.50	–	67.67	50.79	32.20	77.31	59.47	39.20	–
	H_0	m	0.80	0.80	1.80	2.23	2.00	–	0.93	2.23	2.30	1.20	2.74	2.79	–
	C'_c	–	0.2768	0.3025	0.2511	0.2855	0.2685	0.2769	0.3978	0.3513	0.3567	0.3638	0.3745	0.3933	0.3729
	c_t	yr^{-1}	2.4395	4.2173	0.5176	0.8948	0.5432	1.7225	9.9234	15.0868	27.6272	9.0287	10.8582	15.4842	14.6681
	ε_{MB}	–	0.2567	0.2294	0.3024	0.2627	0.4048	0.2912	0.1017	0.0684	0.0697	0.0947	0.1310	0.1208	0.0977
	t_1	yr	0.0027	0.0027	0.0411	0.0411	0.0411	–	0.0795	0.0740	0.0685	0.0493	0.0384	0.0329	–
	R^2	–	0.9605	0.9738	0.9951	0.9842	0.9849	–	0.9121	0.9134	0.8995	0.8241	0.9093	0.8957	–

(*To be continued on the next page*)

(*Continued*)

Model	Para.	Unit	LFWC-MSW					Average	HFWC-MSW						Average
			CARs		DTBE				ZJU-CELL1			ZJU-CELL2			
			CAR1	CAR2	L1	L2	L3		L1	L2	L3	L1	L2	L3	
Gao et al. (2017) [30]	σ_{v0}	kPa	1.27	1.38	8.26	7.03	6.63	–	3.43	8.44	9.30	3.72	8.92	10.13	–
	σ_v	kPa	1.27	1.38	8.26	7.03	6.63	–	3.43	8.44	9.30	3.72	8.92	10.13	–
	$\Delta\sigma$	kPa	150.00	50.00	59.82	45.76	32.50	–	67.67	50.79	32.20	77.31	59.47	39.20	–
	σ_r	kPa	151.27	51.38	68.08	52.79	39.13	1.00	71.10	59.23	41.50	81.03	68.39	49.33	1.00
	H_0	m	0.80	0.80	1.80	2.23	2.00	–	0.93	2.23	2.30	1.20	2.74	2.79	–
	C'_c	–	0.2768	0.3025	0.2511	0.2855	0.2685	0.2769	0.3978	0.3523	0.3567	0.3638	0.3745	0.3933	0.3731
	t_1	yr	0.0027	0.0027	0.0411	0.0411	0.0411	–	0.0795	0.0740	0.0685	0.0493	0.0384	0.0329	–
	$\varepsilon^*_{MB}(\sigma_r)$	yr^{-1}	0.1091	0.1204	0.2328	0.1970	0.3210	0.5353	0.0484	0.0480	0.0535	0.0486	0.0876	0.0882	0.2276
	C'_{c0}-$C'_{c\infty}$	–	–	–	–	–	–	0.2040	–	–	–	–	–	–	0.0916
	c_t	yr^{-1}	2.4395	4.2173	0.5176	0.8948	0.5432	1.7225	9.9234	15.0868	27.6272	9.0284	10.8583	15.4842	14.6681
	R^2	–	0.9605	0.9738	0.9951	0.9845	0.9849	–	0.9121	0.9134	0.8995	0.8241	0.9093	0.8957	–

Table 2 Weight of the four indicators based on the datasets from CARs and DTBE

Model	Matrix **X**				Matrix **R**			
	$\overline{N}$	$\overline{R^2}$	$\overline{\varepsilon_{ex}}$	$\overline{\text{RMSE}}$	$\overline{N}$	$\overline{R^2}$	$\overline{\varepsilon_{ex}}$	$\overline{\text{RMSE}}$
Logarithmic model [10]	3	0.9737	0.6142	0.0330	1.0000	0.1476	0.8769	0.8578
Power model [29]	3	0.9703	1.0000	0.1066	1.0000	0.0000	0.0000	0.0000
Hyperbolic model [7]	3	0.9719	0.6673	0.0293	1.0000	0.0677	0.7566	0.9006
Machado et al. (2009) [4]	4	0.9733	0.6221	0.0402	0.5000	0.1309	0.8593	0.7733
Gourc et al. (2010) [2]	4	0.9915	0.5734	0.0208	0.5000	0.9279	0.9700	1.0000
Sowers et al. (1973) [1]	4	0.9911	0.5602	0.0238	0.5000	0.9139	1.0000	0.9652
Marques et al. (2003) [26]	5	0.9931	0.5484	0.0912	0.0000	1.0000	0.9731	0.1791
Chen et al. (2010) [3]	3	0.9797	0.5435	0.0442	1.0000	0.4112	0.9619	0.7275
Gao et al. (2017) [30]	4	0.9798	0.5435	0.0333	0.5000	0.4139	0.9619	0.8541
Entropy vector **H**					0.9206	0.8154	0.9447	0.9170
Entropy-based weight: **W**=*f*(**H**)					0.1973	0.4590	0.1374	0.2063

computed by using the primary settlement component in eq. (1), or/and can be estimated based on the relationship between C'_c and waste compressibility index (*WCI*) in the absence of measured data [17]. t_2 can be determined from an inflexion of strain-time curve or/and a decrease in leachate *COD*. $C'_{\alpha 1}$ can be determined by fitting the settlement data or estimated from the relationships of $C'_{\alpha 1}$ vs. *WCI* or $C'_{\alpha 1}$ vs. (cellulose + hemicellulose) / lignin [18].

The value of k in Gourc et al. [2] can be determined by (1) exponential regression of *COD* on time [18], or/and (2) computing from biogas generation data via the following equation:

$$k = \frac{\ln(2)}{t_{1/2} - t_2}, \tag{23}$$

where $t_{1/2}$ is the time when half of the total biogas is generated.

The value of ε_{BIO} in Gourc et al. [2] can be determined by using the following equation:

$$\varepsilon_{BIO} = \alpha_m \cdot \frac{\gamma_d}{\gamma_{so}} \cdot \frac{m_{so}}{m_d}, \tag{24}$$

where γ_d is the dry unit weight of MSW at the beginning of secondary settlement [$\gamma_d = \gamma_{do}/(1-\varepsilon_p)$], γ_{so} is the dry unit weight of organic matter, m_{so} is the dry mass of organic matter, m_d is the dry mass of MSW, and α_m is a correction factor. The values of α_m calculated from the datasets of CARs and DTBE are listed in Table 4.

$C'_{\alpha 2}$ in Sowers et al. [1] can be determined by fitting the measured settlement data, and $C'_{\alpha 3}$ can be slightly larger than $C'_{\alpha 1}$. t_3 in Sowers et al. [1] can be estimated through a dual-model approach presented in Bareither et al. [18], where the secondary compression computed by Sowers et al. [1] is equal to that computed by Gourc et al. [2] when $t = t_3$, which

Table 3 Settlement model evaluation for LFWC-MSW

Model	$\overline{N}$		$\overline{R^2}$		$\overline{\varepsilon_{ex}}$		$\overline{\text{RMSE}}$		Comprehensive score
	Weight	Score	Weight	Score	Weight	Score	Weight	Score	
Logarithmic model [10]		1.0000		0.9805		0.8132		0.6300	0.8890
Power model [29]		1.0000		0.9771		0.2188		0.1949	0.7161
Hyperbolic model [7]		1.0000		0.9786		0.7735		0.7089	0.8990
Machado et al. (2009) [4]		0.7500		0.9801		0.8994		0.5164	0.8279
Gourc et al. (2010) [2]	0.1973	0.7500	0.4590	0.9983	0.1374	0.9726	0.2063	1.0000	0.9461
Sowers et al. (1973) [1]		0.7500		0.9980		1.0000		0.8742	0.9238
Marques et al. (2003) [26]		0.6000		1.0000		0.9462		0.2278	0.7544
Chen et al. (2010) [3]		1.0000		0.9865		0.9431		0.4704	0.8767
Gao et al. (2017) [30]		0.7500		0.9866		0.9431		0.6240	0.8591

Table 4 Value of α_m based on the datasets from CARs and DTBE

Compression Test	ε_{BIO}	R^2	γ_d (kN/m^3)	γ_{so} (kN/m^3)	m_{so}/m_d	α_m	$\overline{\alpha_m}$
CAR1	0.1382	0.999	3.90	13.46	0.626	0.762	
CAR2	0.1072	0.999	3.16	13.46	0.626	0.729	
DTBE-L1	0.1703	0.991	8.94	13.40	0.504	0.506	0.663
DTBE-L2	0.1294	0.990	6.64	13.40	0.504	0.518	
DTBE-L3	0.1900	0.978	6.33	13.40	0.504	0.798	

is expressed as

$$C'_{\alpha 1}\lg\left(\frac{t_3}{t_1}\right)+\varepsilon_{BIO}=C'_{\alpha 1}\lg\left(\frac{t_2}{t_1}\right)+C'_{\alpha 2}\lg\left(\frac{t_3}{t_2}\right). \quad (25)$$

6 Assessment of settlement models for HFWC-MSW

6.1 Large-scale compression test of HFWC-MSW in ZJU-CELLs

A large geotechnical model test was constructed in Zhejiang University, China, to investigate the compressive behavior of HFWC-MSW. The test model is in the size of 15.0 m×5.0 m ×7.5 m, and was divided into three cells by using two vertical gates.

ZJU-CELL1 is one of the three test cells, which has the size of 5.0 m×5.0 m×7.5 m. It was filled with fresh MSW obtained from a waste transfer station in Hangzhou, China. The food waste content and paper content were 59.4% (33.9%) and 13.5% (16.8%), respectively, on wet (dry) mass basis. The MSW was filled into the cell by layers and each layer was compacted by using a steel block. Three settlement plates were installed into the cell which divided the whole waste into three layers- L1, L2 and L3 from bottom to top, with their initial thicknesses of 0.93, 2.23 and 2.30 m, and the initial unit weights of 7.37, 7.58 and 8.44 kN/m^3, respectively. The initial vertical stress σ_{v0} was calculated as 3.43, 8.44 and 9.30 kPa for L1, L2 and L3, respectively. 15 d after the waste filling, a layer of gravel, which corresponded to a total vertical stress of 32.20 kPa, was applied to the top of the waste layer. The additional vertical stress $\Delta\sigma_v$ was calculated as 67.67, 50.79 and 32.20 kPa for L1, L2 and L3, respectively. Detailed description of ZJU-CELL1 can be found in Zhan et al. [21]. The daily settlements measured by using each plate are shown in Figure 7(a). t_1 was determined as 29, 27, 25 d, respectively, for each layer via FORE method and t_2 was determined as 38, 36, 36 d respectively based on leachate *COD* analysis. It should be noted that the rapid development of settlement during the days 32–39 was mainly attributed to an increase in effective stress caused by the drawdown of leachate level. Therefore, in the following analysis, the secondary compression curves were amended by removing the compression strains induced by leachate drawdown.

ZJU-CELL2 was another test cell, which has the size of 5.0 m×4.2 m×7.5 m. The food waste and paper contained in the MSW were 55.0% (30.8%) and 15.7% (18.5%) respectively on wet (dry) mass basis. The filling process of waste into ZJU-CELL2 was similar to that of ZJU-CELL1, and the settlement of the three waste layers, named as L1, L2 and L3, was also measured. The initial thicknesses of L1, L2 and L3 were 1.20, 2.74 and 2.79 m, respectively, and their initial unit weights were 6.21, 6.51 and 7.26 kN/m^3, respectively. The calculated initial vertical stress σ_{v0} subjected to L1, L2 and L3 were 3.72, 8.92 and 10.13 kPa, respectively. The place-

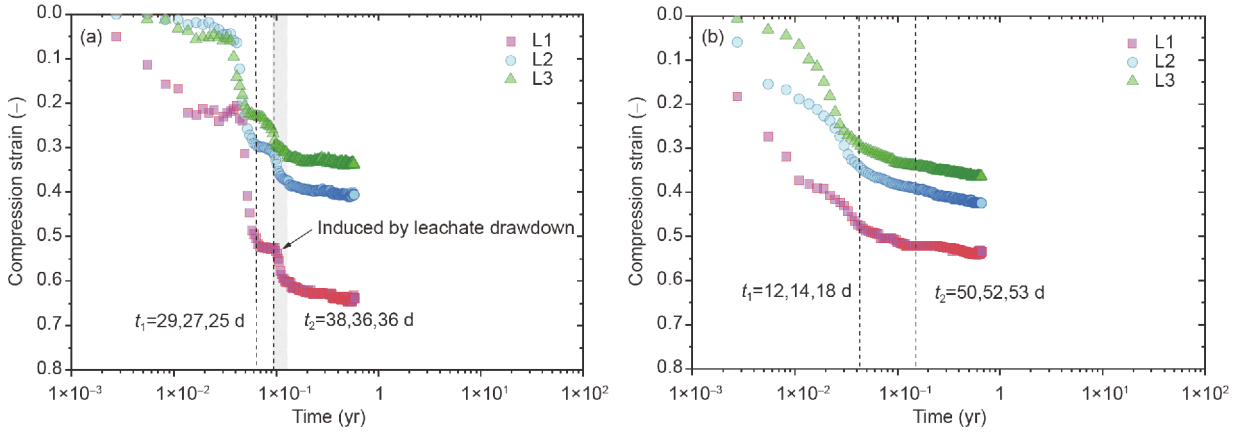

Figure 7 Cumulative compression strain versus time for (a) ZJU-CELL1 and (b) ZJU-CELL2.

ment of the top gravel layer was completed 10 d after waste filling, corresponding to a total applied stress of 39.20 kPa. Then the calculated additional vertical stress $\Delta\sigma_v$ subjected to L1, L2 and L3 were 77.31, 59.47 and 39.20 kPa, respectively. Detailed description of ZJU-CELL2 can be found in Xu [34] and Zhan et al. [69]. The daily settlements measured by each plate are shown in Figure 7(b). t_1 was determined as 18, 14, 12 d via FORE method and t_2 was determined as 53, 52, 50 d based on the analysis of *COD* content in leachate.

6.2 Fitting, prediction and simulation of HFWC-MSW settlement

The compression strain fitted and predicted by the nine settlement models based on the datasets from ZJU-CELL1 and ZJU-CELL2 are shown in Figure 8. The logarithmic model obtained the worst fitting results, but its predicted settlement seemed reasonable. The power model fitted well for the measured data, but highly overestimated the settlement beyond the measured data. The models proposed by Machado et al. [4] and Gourc et al. [2] exhibited similar fitting and predicting performances, and their estimated settlement increased linearly with the logarithmic time. The measured data were best fitted and predicted by the hyperbolic model and the models proposed by Sowers et al. [1] and Marques et al. [26].

The settlement data from ZJU-CELL1 and ZJU-CELL2 were also simulated by the nine settlement models using the average optimized parameters, the results are shown in Figure 9. The primary compression strain was well fitted in the results predicted by all the models, which indicated that the primary compression strain calculated by using C'_c obtained from ZJU-CELL1 and ZJU-CELL2 has a minor variation. In the simulation of the secondary compression, the hyperbolic model and the models proposed by Sowers et al. [1] and Marques et al. [26] exhibited poor performance. Overall, the models proposed by Machado et al. [4] and Gourc et al. [2] performed eminently among the nine models, their simulation results conformed to the compression behaviors of HFWC-MSW at different depths.

6.3 Recommendation of settlement models for HFWC-MSW

Based on the above analysis, the information matrix (**X**) which contains the values of the four indicators for all the nine models was obtained and is presented in Table 5. By using the datasets of ZJU-CELL1 and ZJU-CELL2, the model proposed by Marques et al. [26] was shown to have the best fitting performance ($\overline{R^2} = 0.9568$), and the logarithmic model was found to perform the worst ($\overline{R^2} = 0.3861$). The average compression strains extrapolating to 100 years ($\overline{\varepsilon_{ex}}$) obtained from all models were in the range of 0.4194–0.6577. The large values were obtained by the power model and the models proposed by Machado et al. [4] and Gourc et al. [2], whose fitting curves did not well conform to the compression behaviors of HFWC-MSW. The long-term compression strain predicted by Marques et al. [26] was employed as the referencing value in the evaluation of prediction performance for all models, since this model had the best fitting performance with measured data and its prediction results can also well depict the compression behaviors of HFWC-MSW. When using the average optimized parameters, the models proposed by Machado et al. [4] and Gourc et al. [2] had good simulation performances ($\overline{\text{RMSE}} < 0.022$).

The entropy-based weight of $\overline{N}$, $\overline{R^2}$, $\overline{\varepsilon_{ex}}$ and $\overline{\text{RMSE}}$ were obtained as 0.2873, 0.1796, 0.1838 and 0.3493, respectively, as shown in Table 5. By using the entropy-based weight, the comprehensive score was calculated for each settlement model, and is presented in Table 6. The evaluation result shows that the hyperbolic model and the model proposed by Chen et al. [3] obtained the highest comprehensive score

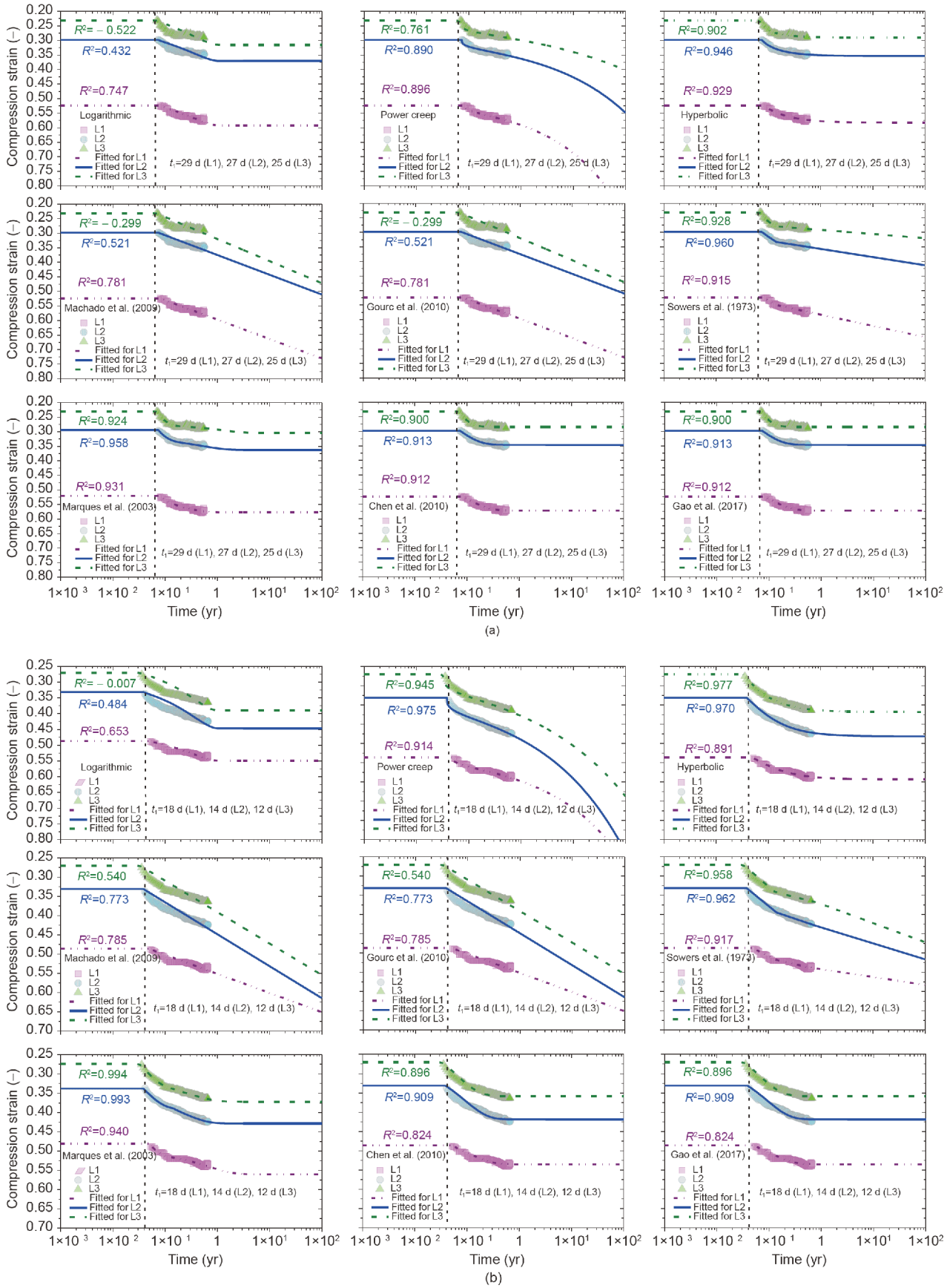

Figure 8 Fitted and predicted compression strains for (a) ZJU-CELL1 and (b) ZJU-CELL2.

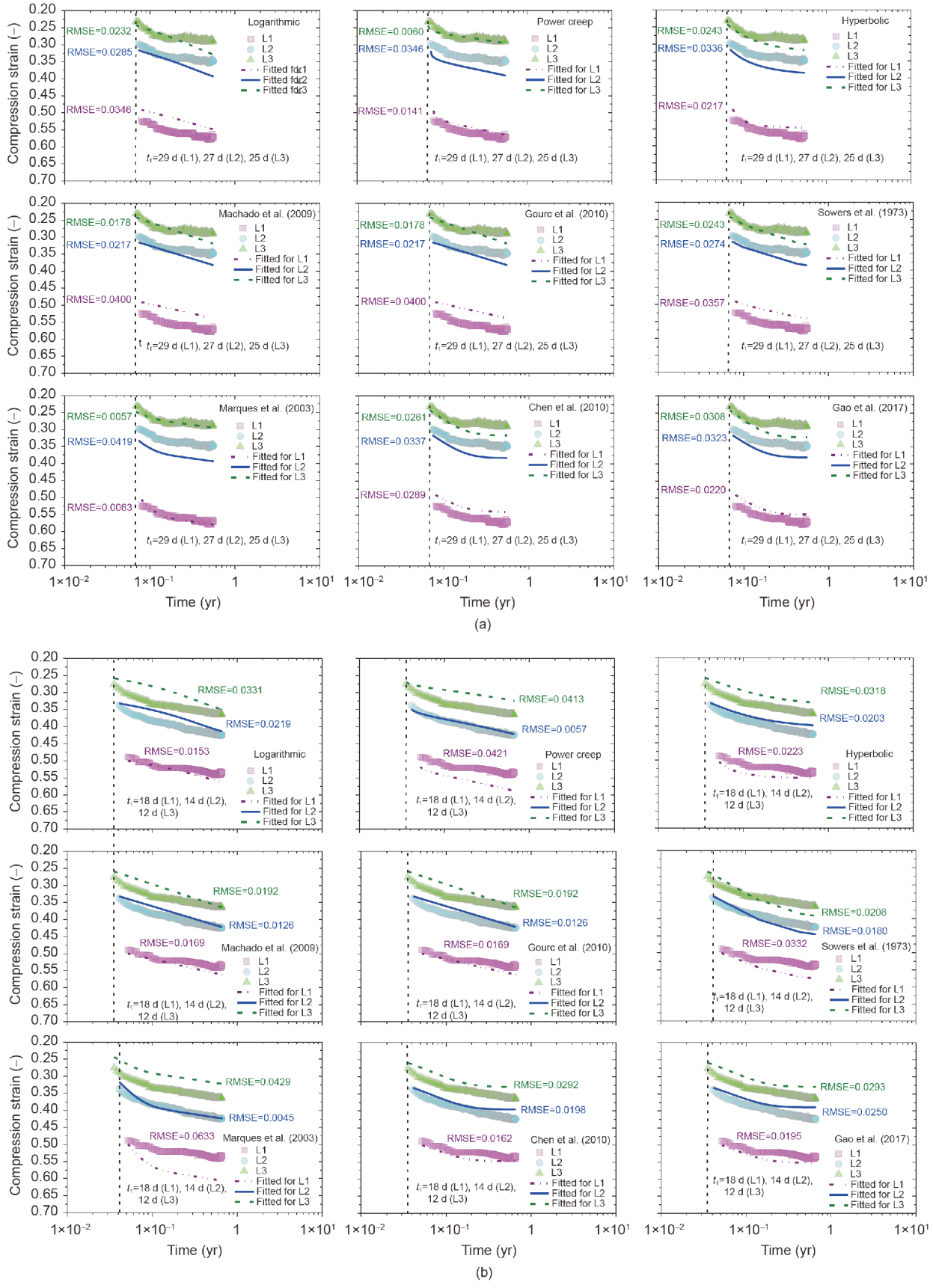

Figure 9 Simulated compression strains by using average value of optimized parameters for (a) ZJU-CELL1 and (b) ZJU-CELL2.

Table 5 Weight of the four indicators based on the datasets from ZJU-CELL1 and ZJU-CELL2

Model	Matrix **X**				Matrix **R**			
	$\overline{N}$	$\overline{R^2}$	$\overline{\varepsilon_{ex}}$	$\overline{\text{RMSE}}$	$\overline{N}$	$\overline{R^2}$	$\overline{\varepsilon_{ex}}$	$\overline{\text{RMSE}}$
Logarithmic model [10]	3	0.3861	0.4441	0.0261	1.0000	0.0000	0.9567	0.2184
Power model [29]	3	0.8968	0.6577	0.0240	1.0000	0.8948	0.0000	0.5736
Hyperbolic model [7]	3	0.9358	0.4284	0.0257	1.0000	0.9632	0.9731	0.2881
Machado et al. (2009) [4]	4	0.5666	0.5889	0.0214	0.5000	0.3163	0.3083	1.0000
Gourc et al. (2010) [2]	4	0.5666	0.5889	0.0214	0.5000	0.3163	0.3083	1.0000
Sowers et al. (1973) [1]	5	0.9398	0.4940	0.0265	0.0000	0.9702	0.7331	0.1455
Marques et al. (2003) [26]	5	0.9568	0.4344	0.0274	0.0000	1.0000	1.0000	0.0000
Chen et al. (2010) [3]	3	0.8924	0.4194	0.0257	1.0000	0.8870	0.9327	0.2923
Gao et al. (2017) [30]	4	0.8924	0.4194	0.0265	0.5000	0.8870	0.9327	0.1536
Entropy vector **H**					0.8619	0.9137	0.9116	0.8321
Entropy-based weight: **W**=*f*(**H**)					0.2873	0.1796	0.1838	0.3493

Table 6 Settlement model evaluation for HFWC-MSWs

Model	$\overline{N}$		$\overline{R^2}$		$\overline{\varepsilon_{ex}}$		$\overline{\text{RMSE}}$		Comprehensive score
	Weight	Score	Weight	Score	Weight	Score	Weight	Score	
Logarithmic model [10]		1.0000		0.4035		0.9681		0.8190	0.8238
Power model [29]		1.0000		0.9372		0.4900		0.8924	0.8574
Hyperbolic model [7]		1.0000		0.9780		0.9785		0.8325	0.9336
Machado et al. (2009) [4]		0.7500		0.5922		0.6158		1.0000	0.7843
Gourc et al. (2010) [2]	0.2873	0.7500	01796	0.5922	0.1838	0.6158	0.3493	1.0000	0.7843
Sowers et al. (1973) [1]		0.6000		0.9822		0.8595		0.8054	0.7881
Marques et al. (2003) [26]		0.6000		1.0000		1.0000		0.7796	0.8081
Chen et al. (2010) [3]		1.0000		0.9326		0.9627		0.8333	0.9228
Gao et al. (2017) [30]		0.7500		0.9326		0.9627		0.8069	0.8418

(S^*>0.92), suggesting an outstanding performance among all the nine models. These two models require fewer optimization parameters to be determined and have higher accuracy. Moreover, it is more appropriate to use a function without phase transitional times to describe the secondary compression behavior of HFWC-MSW, since it is hard to determine the transitional time from phase I to II. Therefore, these two models, hyperbolic and Chen et al. [3], were recommended as ideal models for predicting the settlement at HFWC-MSW landfills.

The parameters in the hyperbolic and Chen et al. [3] models can be obtained in the following ways. C'_c can be computed via the primary settlement component of Eq.(1) with settlement data, or/and estimated by using the relationship between C'_c and *WCI* in the absence of measured data. The reference values of secondary compression parameters in hyperbolic model ($\varepsilon_{S,ult}$ and ρ_0) and Chen et al. [3] model (ε_{MB} and c_t) were summarized in Table 7. They were obtained from the fitting of the compression test datasets of HFWC-MSWs in the literatures. The waste information and test condition in each literature were also included in Table 7, as a reference when determining these model parameters.

7 Conclusions

In this study, the settlement behaviors of both HFWC-MSW and LFWC-MSW were characterized based on a large number of compression curves summarized from references. In addition, the applicability of nine published models to predict the settlement at both HFWC-MSW and LFWC-MSW landfills were evaluated by using the datasets of four large-scale model tests obtained from references. The main findings are as follows.

The average values of primary compression ratio (C'_c) are 0.33 and 0.22 for fresh HFWC-MSW and fresh LFWC-MSW, respectively, and are both approximately 0.21 for aged HFWC-MSW and aged LFWC-MSW. The larger C'_c value of fresh HFWC-MSW is mainly attributed to the release of a large amount of intra-particle water contained in food waste.

Table 7 Summary of parameters in the models recommended for HFWC-MSW

Literatures	Waste description	Test condition	Chen et al. (2010) model		R^2	Hyperbolic model		R^2
			ε_{MB}	c_t (yr^{-1})		$\varepsilon_{S,ult}$	ρ_0 (m/yr)	
Peng [58]	FWC=21%[a)] DO=61%[b)] w_{d0}=49.3% γ_{d0}=2.93 kN/m^3 H_0=1.76 m	$\Delta\sigma$=17.28 kPa	0.2498	3.5723	0.990	0.3578	1.6746	0.983
Xie et al. [8]	DO=50% H_0=0.235 m	$\Delta\sigma$=3 kPa	0.1004	3.7093	0.985	0.1370	0.0815	0.990
	DO=65% H_0=0.235 m	$\Delta\sigma$=3 kPa	0.0654	5.4992	0.977	0.0831	0.0795	0.990
Jin [61]	(AMF) FWC=75% DO=87% w_{d0}=138.1% γ_{d0}=2.37 kN/m^3 H_0=0.63 m	Flushing; Aerobic & Anaerobic stages; Supplied air = 0.617 L d^{-1} Mg^{-1}	0.2448	18.0863	0.994	0.3059	3.4377	0.991
	(AMR1) FWC=75% DO =87% w_{d0}=170.3% γ_{d0}=2.02 kN/m^3 H_0=0.66 m	Leachate recirculation; Aerobic & Anaerobic stages; Supplied air = 0.617 L d^{-1} Mg^{-1}; pH=6.4–7.2	0.1997	22.4540	0.875	0.2304	4.4947	0.930
	(ASF) FWC=61% DO =71% w_{d0}=203% γ_{d0}=1.80 kN/m^3 H_0=0.64 m	Flushing; Aerobic & Anaerobic stages; Supplied air = 0.617 L d^{-1} Mg^{-1}	0.2176	67.9550	0.966	0.2388	14.6762	0.962
	(ASR) FWC=61% DO =71% w_{d0}=203% γ_{d0}=1.76 kN/m^3 H_0=0.64 m	Leachate recirculation; Aerobic & Anaerobic stages; Supplied air = 0.617 L d^{-1} Mg^{-1}; pH=6.4–7.2	0.2960	8.8982	0.946	0.4053	1.9436	0.952
	(NMR) FWC=75% DO =87% w_{d0}=138.1% γ_{d0}=2.18 kN/m^3 H_0=0.73 m	Leachate recirculation; Constant anaerobic stage; Supplied air = 0.617 L d^{-1} Mg^{-1}; pH=6.4–7.2	0.2378	43.2550	0.954	0.2697	10.6806	0.973
Chen et al. [63]	FWC=25% DO =40% w_{d0}=50% γ_{d0}=2.0 kN/m^3 H_0=1 m		0.3000	2.3615	0.966	0.4000	0.6916	0.951
Xu [34]	(A1) FWC=37.7% DO =58.3% w_{d0}=167.8% γ_{d0}=3.39 kN/m^3 H_0=0.85 m	$\Delta\sigma$=10 kPa; T=(40±3)°C; Anaerobic degradation	0.2800	4.8623	0.760	0.3100	1.5576	0.894
	(A2) FWC=37.7% DO =58.3% w_{d0}=167.8% γ_{d0}=3.23 kN/m^3 H_0=0.85 m	$\Delta\sigma$=10 kPa; T=(40±3)°C; Anaerobic degradation	0.3200	8.7605	0.818	0.3500	3.0114	0.923

(*To be continued on the next page*)

(*Continued*)

Literatures	Waste description	Test condition	Chen et al. (2010) model		R^2	Hyperbolic model		R^2
			ε_{MB}	c_t (yr^{-1})		$\varepsilon_{S,ult}$	ρ_0 (m/yr)	
	(ZJU-CELL1) (L2) *FWC*=33.9% *DO*=55.8% w_{d0}=235.6% γ_{d0}=2.26 kN/m^3 H_0=2.23 m	$\Delta\sigma$=50.79 kPa; Leachate recirculation	0.0684	15.0868	0.913	0.0791	4.0763	0.946
	(ZJU-CELL2) (L2) *FWC*=30.8% *DO*=57.0% w_{d0}=165.3% γ_{d0}=2.45 kN/m^3 H_0=2.74 m	$\Delta\sigma$=59.47 kPa	0.1310	10.8582	0.909	0.1107	0.7989	0.970
Zhao [60]	*FWC*=24.4% *DO*=32.4% γ_{d0}=8.36 kN/m^3 H_0=0.5 m	$\Delta\sigma$=100 kPa	0.0679	6.0852	0.988	0.0807	0.2628	0.994
	FWC=24.4% *DO*=32.4% γ_{d0}=8.36 kN/m^3 H_0=0.5 m	$\Delta\sigma$=200 kPa	0.0885	5.1465	0.988	0.1093	0.2534	0.998
Range	–	–	0.0679–0.3200	2.3615–67.9550	0.760–0.994	0.0791–0.4053	0.0795–14.6762	0.894–0.998
(Average)	–	–	0.1912	15.1060	0.935	0.2312	3.1814	0.963

a) *FWC* is food waste content of waste samples (dry mass basis); b) *DO* is content of degradable organic matter (dry mass basis).

In the secondary compression, the starting time of transitional phase (t_1) for HFWC-MSW is close to that of LFWC-MSW, suggesting comparative primary compression durations for both MSWs. The starting times of active biodegradation phase (t_2) and residual phase (t_3) are both earlier for HFWC-MSW than that for LFWC-MSW, which is associated with the better degradation conditions and lower content of slowly-decomposed materials for HFWC-MSW. The slopes in the strain-logarithmic time curves with respect to the three secondary compression phases are characterized as "slight-steep-slight" for LFWC-MSW and "moderate-moderate-slight" for HFWC-MSW. It is feasible to separate the secondary compression into three phases for LFWC-MSW; however, it is difficult to distinguish the first two phases for HFWC-MSW.

An entropy method was built to evaluate the performance and applicability of nine published settlement models. In this method, the following four criterions are considered: (1) the computational simplicity assessed by the number of independent optimized parameters; (2) the fitting performance assessed by the determination coefficient based on the measured data; (3) the prediction performance assessed by the extrapolated long-term settlement beyond the measured data; (4) the parametric stability assessed by the simulation performance using average value of optimized parameters. After a comprehensive assessment with this method, the models proposed by Sowers et al. [1] and Gourc et al. [2] are recommended for predicting the settlement at LFWC-MSW landfills, and the hyperbolic model and the Chen et al. [3] model are recommended for HFWC-MSW landfills.

This work was supported by the National Basic Research Program of China (Grant No. 2012CB719802), the National Natural Science Foundation of China (Grant Nos. 51708508, 41402249), the Zhejiang Provincial Natural Science Foundation of China (Grant Nos. LY17E080021, LY15E080021), and the Science Technology Department of Zhejiang Province (Grant No. 2019C03107). The authors also want to express their deep thanks to Prof. William Powrie and Dr. Richard Beaven from University of Sonthampton for their constructive comments.

1 Sowers G F. Settlement of waste disposal fills. In: Proceedings of the 8th International Conference on Soil Mechanics, and Foundation on Engineering. Moscow, 1973. 207–210
2 Gourc J P, Staub M J, Conte M. Decoupling MSW settlement into mechanical and biochemical processes-Modelling and validation on large-scale setups. Waste Manage, 2010, 30: 1556–1568
3 Chen Y M, Ke H, Fredlund D G, et al. Secondary compression of Municipal solid wastes and a compression model for predicting settlement of municipal solid waste landfills. J Geotech Geoenviron Eng, 2010, 136: 706–717
4 Machado S L, Carvalho M. Constitutive model for municipal solid waste incorporating mechanical creep and biodegradation-induced compression. Waste Manage, 2009, 30: 11–22
5 Babu S G L, Reddy K R, Chouskey S K, et al. Prediction of long-term municipal solid waste landfill settlement using constitutive model. Practice Periodical Hazardous, Toxic, Radioactive Waste Manage,

2010, 14: 139–150
6 Laner D, Crest M, Scharff H, et al. A review of approaches for the long-term management of municipal solid waste landfills. Waste Manage, 2012, 32: 498–512
7 Ling H I, Leshchinsky D, Mohri Y, et al. Estimation of municipal solid waste landfill settlement. J Geotechnical GeoEnviron Eng, 1998, 124: 21–28
8 Xie Q. A study on the settlement of sanitary landfill of municipal solid waste (in Chinese). Dissertation for Doctoral Degree. Chongqing: Chongqing University, 2004
9 Liu C N, Chen R H, Chen K S. Unsaturated consolidation theory for the prediction of long-term municipal solid waste landfill settlement. Waste Manag Res, 2006, 24: 80–91
10 Yen B C, Scanlon B. Sanitary landfill settlement rates. J Geotech Eng Div, 1975, 101: 475–487
11 Park H I, Lee S R. Long-term settlement behavior of landfills with refuse decomposition. Res Manage Technol, 1997, 24: 159–165
12 Yuen S T, Styles J R. Settlement and characteristics of waste at a municipal solid waste landfill in Melbourne. In: Proceedings of the International Conference on Geotechnical and Geological Engineering. Melbourne, 2000
13 Olivier F, Gourc J P. Hydro-mechanical behavior of municipal solid waste subject to leachate recirculation in a large-scale compression reactor cell. Waste Manage, 2007, 27: 44–58
14 Swati M, Joseph K. Settlement analysis of fresh and partially stabilised municipal solid waste in simulated controlled dumps and bioreactor landfills. Waste Manage, 2008, 28: 1355–1363
15 Ivanova L K, Richards D J, Smallman D J. The long-term settlement of landfill waste. Water Resour Manage, 2008, 161: 121–133
16 Bareither C A, Breitmeyer R J, Benson C H, et al. Deer track bioreactor experiment: Field-scale evaluation of municipal solid waste bioreactor performance. J Geotech Geoenviron Eng, 2012, 138: 658–670
17 Bareither C A, Benson C H, Edil T B. Compression behavior of municipal solid waste: Immediate compression. J Geotech Geoenviron Eng, 2012, 138: 1047–1062
18 Bareither C A, Benson C H, Edil T B. Compression of municipal solid waste in bioreactor landfills: Mechanical creep and biocompression. J Geotech Geoenviron Eng, 2013, 139: 1007–1021
19 Fei XC, Zekkos D. Factors influencing long-term settlement of municipal solid waste in laboratory bioreactor landfill simulators. J Hazard Toxic Radioact Waste, 2013, 17: 259–271
20 Heshmati R A A, Mokhtari M, Shakiba Rad S. Prediction of the compression ratio for municipal solid waste using decision tree. Waste Manag Res, 2014, 32: 64–69
21 Zhan L T, Xu H, Chen Y M, et al. Biochemical, hydrological and mechanical behaviors of high food waste content MSW landfill: Preliminary findings from a large-scale experiment. Waste Manage, 2017, 63: 27–40
22 Zhan L T, Xu H, Chen Y M, et al. Biochemical, hydrological and mechanical behaviors of high food waste content MSW landfill: Liquid-gas interactions observed from a large-scale experiment. Waste Manage, 2017, 68: 307–318
23 Bjarngard A, Edgers L. Settlement of municipal solid waste landfills. In: Proceedings of the 13th Annual Madison Waste Conference. Madison, 1990. 192–205
24 Hossain M S, Gabr M A. Prediction of municipal solid waste landfill settlement with leachate recirculation. In: Proceedings of the GeoFrontiers 2005 Congress. Austin, 2005. 1–14
25 Sivakumar Babu G L, Reddy K R, Chouksey S K. Constitutive model for municipal solid waste incorporating mechanical creep and biodegradation-induced compression. Waste Manage, 2010, 30: 11–22
26 Marques A C M, Filz G M, Vilar O M. Composite compressibility model for municipal solid waste. J Geotechnical GeoEnviron Eng, 2003, 129: 372–378
27 Shi J Y, Qian X D, Liu X D, et al. The behavior of compression and degradation for municipal solid waste and combined settlement calculation method. Waste Manage, 2016, 55: 154–164
28 Park H I, Park B, Lee S R, et al. Parameter evaluation and performance comparison of MSW settlement Prediction models in various landfill types. J Environ Eng, 2007, 133: 64–72
29 Edil T B, Ranguette V J, Wuellner W W. Settlement of municipal refuse. In: Proceedings of the Symposium on Geotechnics of Waste Fills—Theory and Practice. STP 1070. West Conshohocken: ASTM Special Technical Publication, 1990. 225–239
30 Gao W, Bian X C, Xu W J, et al. An equivalent-time-lines model for municipal solid waste based on its compression characteristics. Waste Manage, 2017, 68: 292–306
31 Siddiqui A A, Powrie W, Richards D J. Settlement characteristics of mechanically biologically treated wastes. J Geotech Geoenviron Eng, 2013, 139: 1676–1689
32 Bareither C A, Kwak S. Assessment of municipal solid waste settlement models based on field-scale data analysis. Waste Manage, 2015, 42: 101–117
33 Bareither C A. Compression behavior of solid waste. Dissertation for Doctoral Degree. Madison: University of Wisconsin-Madison, 2010
34 Xu H. Large-scale experiment on biochemo-hydro-mechanical behaviors of high-food- waste-conetnt MSW and applications (in Chinese). Dissertation for Doctoral Degree. Hangzou: Zhejiang University, 2016
35 Liao Z Q, Shi J Y, Mao J. Experimental study and mechanism analysis of primary compression index of MSW (in Chinese). J Hohai Univ, 2007, 35: 326–329
36 Sun H J, Liang L, Zhao L H, et al. Experimental analysis of primary compression settlement of municipal solid waste landfill (in Chinese). Ind Const, 2009, 39: 84–107
37 Liu J L. Study on compressibility of municipal solid waste and settlement models of landfill (in Chinese). Dissertation for Master Degree. Hangzhou: Zhejiang University, 2010
38 Ke H, Liu J L, Chen Y M, et al. Biodegradation-compression tests on municipal solid waste subjected to different vertical pressures (in Chinese). Chin J Geotech Eng, 2010, 32: 1610–1615
39 Xie Q, Zhang Y X, Zhang J H. Experimental study on the compressibility of stale waste (in Chinese). J Chongqing Jianzhu Univ, 2003, 25: 18–25
40 Vilar O M, Carvalhod M. Mechanical properties of municipal solid waste. J Test Eval, 2004, 32: 209–217
41 Chen Y M, Zhan L T, Wei H Y, et al. Aging and compressibility of municipal solid wastes. Waste Manage, 2009, 29: 86–95
42 Rao S K, Moulton L K, Seals R K. Settlement of refuse landfills. In: Proceedings of the Conference on Geotechnical Practice for Disposal of Solid Waste Materials. Ann Arbor, New York, 1977. 574–598
43 Beaven R P, Powrie W. Determination of hydrogeological and geotechnical properties of refuse using a large compression cell. In: Proceedings of the Sardinia 95, 5th International Landfill Symposium. Cagliari, 1995
44 Wall D K, Zeiss C. Municipal landfill biodegradation and settlement. J Environ Eng, 1995, 121: 214–224
45 Landva A O, Valsangkar A J, Pelkey S G. Lateral earth pressure at rest and compressibility of municipal solid waste. Can Geotech J, 2000, 37: 1157–1165
46 Olivier F, Gourc, J P, Lopez S.et al. Mechanical behavior of solid waste in a fully instrumented prototype compression box. In: Proceedings of the 9th International Waste Management and Landfill Symposium. Cagliari, 2003. 1–12
47 Hossain M S, Gabr M A, Barlaz M A. Relationship of compressibility parameters to municipal solid waste decomposition. J Geotechnical GeoEnviron Eng, 2003, 129: 1151–1158
48 Reddy K R, Gangathulasi J, Parakalla N S, et al. Compressibility and shear strength of municipal solid waste under short-term leachate recirculation operations. Waste Manag Res, 2009, 27: 578–587
49 Reddy K R, Hettiarachchi H, Gangathulasi J, et al. Geotechnical properties of synthetic municipal solid waste. Int J Geotech Eng, 2009, 3: 429–438
50 Reddy K R, Hettiarachchi H, Parakalla N S, et al. Geotechnical

properties of fresh municipal solid waste at Orchard Hills landfill, USA. Waste Manage, 2009, 29: 952–959
51 Stoltz G, Gourc J P. Influence of compressibility of domestic waste on fluid permeability. In: Proceedings of the 11th International Waste Management and Landfill Symposium. Cagliari, 2007. 1–8
52 Stoltz G, Gourc J P, Oxarango L. Characterisation of the physico-mechanical parameters of MSW. Waste Manage, 2010, 30: 1439–1449
53 Gabr M A, Valero S N. Geotechnical properties of municipal solid waste. Geotech Test J, 1995, 18: 241–251
54 Machado S L, Carvalho M F, Vilar O M. Constitutive model for municipal solid waste. J Geotechnical GeoEnviron Eng, 2002, 128: 940–951
55 Xu H, Zhan L, Li H, et al. Time- and stress-dependent model for predicting moisture retention capacity of high-food-waste-content municipal solid waste: based on experimental evidence. J Zhejiang Univ Sci A, 2016, 17: 525–540
56 Fei X C, Zekkos D, Raskin L. An experimental setup for simultaneous physical, geotechnical, and biochemical characterization of municipal solid waste undergoing biodegradation in the laboratory. Geotech Test J, 2014, 37: 1–12
57 Liu J Y, Xu D M, Zhao Y C. Research on settlement of municipal refuse landfill (in Chinese). Soil Environ Sci, 2002, 11: 111–115
58 Peng G X. Settlement of municipal solid waste (in Chinese). Dissertation for Doctoral Degree. Nanjing: Hohai University, 2004
59 Shi J Y, Lei G H, Ai Y B, et al. Settlement calculation method and experimental study of wastes by considering decomposition of organic matter (in Chinese). Rock Soil Mech, 2006, 27: 1673–1677
60 Zhao Y R. Study on the mechanical and biodegradation settlement properties of municipal solid waste (in Chinese). Dissertation for Doctoral Degree. Chongqing: Chongqing University, 2014
61 Jin H. Decomposition of high organic and moisture content municipal solid waste in bioreactor landfills. Dissertation for Master Degree. Toronto: Ryerson University, 2005
62 Liao Z Q. Biodegredation experiment study and mechanism analysis of landfill settlement (in Chinese). Dissertation for Doctoral Degree. Nanjing: Hohai University, 2006
63 Chen J D, Shi J Y, Hu Y D. One-dimensional compression modified method of settlement of landfills and verification of degradation of organic content in solid waste (in Chinese). Rock and Soil Mechanics, 2008, 29: 1797–1801
64 Bareither C A, Benson C H, Edil T B, et al. Abiotic and biotic compression of municipal solid waste. J Geotech Geoenviron Eng, 2012, 138: 877–888
65 Chen Y M, Guo R Y, Li Y C, et al. A degradation model for high kitchen waste content municipal solid waste. Waste Manage, 2016, 58: 376–385
66 Guo R Y. Anaerobic degradation properties of high kitchen waste content municipal solid waste and influences on its engineering behaviors in landfills (in Chinese). Dissertation for Doctoral Degree. Hangzhou: Zhejiang University, 2017
67 Tan T, Inoue T, Lee S. Hyperbolic method for consolidation analysis. J Geotechnical Eng, 1991, 117: 1723–1737
68 Handy R L. First-order rate equations in geotechnical engineering. J Geotech Geoenviron Eng, 2002, 128: 416–425
69 Zhan L T, Xu H, Jiang X M, et al. Use of electrical resistivity tomography for detecting the distribution of leachate and gas in a large-scale MSW landfill cell. Environ Sci Pollut Res, 2019, 26: 20325–20343